Report
P-17-02
June 2017

Two-phase flows during re-saturation of sparsely fractured bedrock and bentonite around canisters for deep storage of spent nuclear fuel

Modelling Task 8 of SKB Task Forces GWFTS and EBS

Benoît Dessirier
Andrew Frampton
Jerker Jarsjö

SVENSK KÄRNBRÄNSLEHANTERING AB

SWEDISH NUCLEAR FUEL
AND WASTE MANAGEMENT CO

Box 3091, SE-169 03 Solna
Phone +46 8 459 84 00
skb.se

SVENSK KÄRNBRÄNSLEHANTERING

ISSN 1651-4416
SKB P-17-02
ID 1586737
June 2017

Two-phase flows during re-saturation of sparsely fractured bedrock and bentonite around canisters for deep storage of spent nuclear fuel

Modelling Task 8 of SKB Task Forces GWFTS and EBS

Benoît Dessirier, Andrew Frampton, Jerker Jarsjö
Department of Physical Geography, Stockholm University

Executive summary

This report presents the numerical modeling work that has been carried out in support of the BRIE experiment at Äspö HRL. The objectives were to determine the effects of fractures and heterogeneity on two-phase air-water flows in the near-canister domain and assess the likely extent of sub-grid scale processes (e.g. bubble trapping, gas dissolution) both in the bentonite buffer envisaged for the KBS-3 repository concept and in the natural sparsely fractured host rock. A particular attention is given to the physical interface between the buffer and the surrounding rock mass and at points where rock fractures intersect this interface.

The approach adopted consists first of scenario and global sensitivity analyses where different sets of modeling assumptions are examined on geometrically simplified 2D models. The configuration includes the tunnel, a deposition hole (first empty then filled by bentonite blocks) intersected by one rock fracture. The first part of analysis compared flow predictions by two-phase flow of air and water as implemented in the simulation code TOUGH2 (EOS3) with a commonly used simplified unsaturated flow description, namely Richards' equation which assumes air is a perfectly mobile bystander, as implemented in TOUGH2 (EOS9). A second part of the analysis investigates different intersection points between the fracture and the deposition hole. Furthermore, we also investigated buffer saturation times and the potential for dissolution of the air introduced with the buffer into the liquid phase which would imply a longer residence time. Also, a detailed analysis based on a site-specific 3D model of the BRIE tunnel was conducted in order to test the capability to capture the wetting dynamics with the available flow representations and characterization data.

The results of the numerical simulations show that for all scenarios the installation of a bentonite buffer can cause considerable de-saturation of the adjacent rock matrix, approximately up to 10 cm into the rock matrix during the first half year for the tested setup (for a deposition hole radius of 15 cm). There are however difficulties to sustain this de-saturation for the duration that was observed in BRIE. The position of the fracture/deposition hole intersections can considerably influence buffer saturation times. It is in fact observed that the aggregated open deposition hole inflow value constrains the wetting time prediction poorly. The local fracture intersections with the deposition hole, on the contrary, and likely the in-plane channeling in these fractures seem to be determinant in order to obtain a reliable buffer saturation time. Analyses of bentonite samples and dismantling photographs helped identify features influencing the wetting process near the bentonite/rock interface, among which previously identified fracture traces along with other possibly stress-related subvertical features.

Richards' equation systematically predicts higher degrees of saturation and shorter saturation times than the model with full two-phase flow representation. The under-prediction made by Richards' equation were relatively small (10–15 %) at lower water saturations (approximately up to 85 % saturation) but it increases as the system approaches saturation; underestimations in times to reach full (or near-full) water saturations were considerable. Uncertainty remains with regards to the amount of air introduced with the buffer that may undergo dissolution to stay in the liquid phase in the vicinity of the canisters for prolonged periods of time and engage in biogeochemical processes, which might be of relevance in the safety assessment.

Sammanfattning

I denna rapport presenteras det numeriska modelleringsarbete som har utförts till stöd för BRIE-experimentet på Äspölaboratoriet. Målsättningarna var att bestämma effekterna av bergsprickor och heterogenitet på tvåfasflöden (av luft-vatten) i domänen nära kapseln, samt att uppskatta den sannolika betydelsen av sub-grid processer (t.ex. immobilisering av gas, upplösning av gas) både i den bentonitbuffert som planeras för KBS3-slutförvarskonceptet och i den naturliga glest sprickiga berggrunden. Särskilt uppmärksammas den fysikaliska gränsytan mellan bufferten och den omgivande bergmassan samt de punkter där bergsprickor möter med denna gränsyta.

Tillvägagångssättet består först av scenario- och globala känslighetsanalyser där olika kombinationer av modelleringsantaganden undersöks på geometriskt förenklade 2D-modeller. Konfigurationen innefattar tunneln och ett deponeringshål (först tomt, sedan fyllt av bentonitblock) som skärs av en bergspricka. Den första delen av analysen jämförde flöde som prognosticerades med en luft-vatten tvåfasflödesbeskrivning som implementerats i simuleringskoden TOUGH2 (EOS3) med en vanligt förekommande förenklad beskrivning av omättat flöde, nämligen Richards ekvation (EOS9 i TOUGH2) som antar att luft är en fullständigt mobil komponent. Den andra delen av analysen undersöker olika skärningspunkter mellan sprickan och deponeringshålet. Vidare undersökte vi även buffertmättnads-tider och potentialen för upplösning i vätskefasen av luft som införts med bufferten. Sådan upplösning skulle innebära en längre uppehållstid. En systematisk analys baserad på en platsspecifik 3D-modell av BRIE-tunneln genomfördes också för att testa förmågan att reproducera vätningsdynamiken med tillgängliga flödesmodeller och karakteriseringsdata.

Resultaten av de numeriska simuleringarna visar för alla scenarier att installationen av en bentonit-buffert kan orsaka omättade förhållanden i den intilliggande bergmatrisen, ungefär upp till 10 cm in i matrisen under det första halvåret för testade förhållanden (med en deponeringshålsradie på 15 cm). Det fanns dock svårigheter att få modellen att bibehålla denna omättnad under den tid som observerades i BRIE. Skärningspunktens läge mellan sprickan och deponeringshålet kan påtagligt påverka buffertmättnadstiderna. Det observeras vidare att det aggregerade inflödet till ett öppet deponeringshål är en dålig indikator för mättnadstider. Däremot verkar de lokala sprickmönstren på deponeringshålets yta och sannolikt kanaliseringgraden i dessa sprickplan vara bestämmande faktorer för att erhålla pålitliga prognoser av buffertmättnadstid. Analyser av bentonitprover och demonteringsfoton bidrog till att identifiera de förhållanden som påverkar mättningsprocessen nära gränsytan mellan bentonit och berg, tillsammans med data över tidigare identifierade sprickmönster och andra eventuellt stressrelaterade subvertikala sprickor.

Richards ekvation förutsäger systematiskt högre mättnadsgrader och kortare mättnadstider än modellen med full tvåfasflödesrepresentation. Den underskattning som gjordes av Richards ekvation var relativt liten (10–15 %) vid lägre vattenmättnad (ungefär upp till 85 % mättnad) men den ökade när systemet närmar sig full mättnad; underskattningen var betydande vad gäller tiden för att uppnå full (eller nästan full) vattenmättnad. Osäkerheten kvarstår med avseende på den mängd luft som införs med bufferten, vilken kan upplösas och stanna kvar i vätskefasen i närheten av kapslarna under lång tid. Detta kan påverka biogeokemiska processer, vilket kan vara av betydelse i säkerhetsbedömningen.

Contents

1 Introduction

1.1 Background

Key open issues related to the phenomena of two-phase flow and transport, and their influence on flow and transport pathways in the canister vicinity, are addressed in this report considering the design of a deep repository proposed by the Swedish Nuclear Fuel and Waste Management Company (SKB). The Task 8 project combined with the BRIE experiments at Äspö Hard Rock Laboratory present a unique opportunity to further investigate many aspects of unsaturated flow phenomena, both in relation to high-profile applications involving repository planning as well as broader concerns within the scientific community.

During the re-saturation phase that follows after the canister installation, unsaturated conditions may prevail in the backfill material and adjacent bedrock for an extended period of time if the re-saturation process is sufficiently slow, which can be the case if a relatively high suction of the bentonite and/or the backfill causes a de-saturation of the ambient rock and fractures. The prevalence of such unsaturated conditions in porous and fractured media generally has a considerable influence on the flow field and thereby also on transport. Specifically, the occurrence of mixed gas-water flows may influence the environment near the deposition holes as well as the physical and biogeochemical processes along the transport pathways from the repository. A comprehensive understanding of two-phase flows is for instance imperative in order to predict the transport of potentially corrosive substances (e.g. sulphide) in the vicinity of the canister; such substances may also alter local hydro-geochemical conditions and impact escape routes for radioactive substances from malfunctioning canisters.

Hence, flow and transport pathways may potentially exist through the bentonite-clay buffer into the surrounding bedrock. Predictive modeling therefore needs to account for properties of, and interactions between both systems. However, such modeling of two-phase flow in a domain containing an interface between an engineered (bentonite-clay) system and a natural (sparsely fractured) bedrock is scientifically challenging. For instance, there are numerous scientific observations of two-phase flow behavior in the soil environment, whereas there are fewer observations for the engineered bentonite-clay buffer (Tong et al. 2010), which is characterized with much lower permeabilities than most natural systems, and fractured bedrock (Liu and Bodvarsson 2001), in which effects of for instance buoyancy and bubble trapping may differ from the soil environment (Jarsjö and Destouni 1998, 2000, Jarsjö et al. 2001).

Furthermore, interactions between the bentonite and bedrock interface have not previously been thoroughly investigated. The well-controlled properties of the engineered systems contrast to the characteristics of the sparsely fractured bedrock that cannot be fully characterized due to its relative inaccessibility to observation. Models must explicitly account for effects of uncertain ambient conditions, and may therefore need to be able to consider both deterministic and stochastic approaches to uncertainty analysis, using for instance (combinations of) scenario analyses (Chasset et al. 2011) and probabilistic frameworks (Frampton 2010). Computational modeling of the interface zone also involves technical and numerical development challenges. Fractured media challenge the assumptions of a single pore space continuum often used while upscaling/parameterizing permeability and capillarity laws. And in the case of bentonite, the multi-level microstructure and the chemical interactions between the water molecules and the clay particles fall clearly out of the classical capillary framework underlying two-phase flow models in porous media. Overall, the uncertainties mentioned above mean that assumptions commonly used in state-of-the-art two-phase flow modeling of classical soil systems may need to be modified for investigations of the interlinked bentonite-sparsely fractured bedrock system, and the robustness to remaining uncertainties needs to be evaluated.

1.2 Objectives

Specific objectives of the SU project are to determine:

[1] Effects of fractures on two-phase flows in the near-canister domain.

[1] Effects of sub-grid scale processes (e.g. bubble trapping, gas dissolution) on predictions of mixed gas-water flows in the near-canister domain.

[2] Impacts of two-phase flows near the canister (addressed in [1] and [2]) on flows in the larger, coupled near-canister domain and adjacent sparsely fractured rock domain.

[3] Re-saturation behavior of fractured rock and improving the understanding of the potential for transport of water and air from rock to bentonite, considering inherent uncertainties (using results from [1], [2] and [3]).

1.3 Scope

To relate to the outline of the task description (Vidstrand et al. 2017), Task 8A has been completed and extended to include the influence of simple unsaturated flow modeling using Richards' equation versus a two-phase/two-component approach and the impact of different fracture intersections on the deposition hole (Chapter 2). The setting of Task 8a was also used to perform a global sensitivity analysis of the time to near buffer saturation, including also an analysis of the potential for dissolution of the air mass initially introduced with the buffer as well as the time to maximum dissolution (Chapter 3). In this report, other subtasks are not strictly followed according to the task description. Rather, key parts of the subtasks are used to address project objectives [1]–[4]. For example, Chapter 4 presents the wetting simulations according to 3D site-specific models of the BRIE site taking in some of the geometrical information released after the completion of the BRIE field campaign, thus corresponding loosely to subtasks 8d2–f2. Chapter 5 presents an unanticipated digression on the analysis of dismantling photographs obtained for BRIE hole 18, trying to gather insight in the rock features that influenced the buffer wetting process. The overall aim is to improve current understanding of unsaturated flow phenomena, considering scales and ambient conditions relevant for the BRIE experiment and Task Force – Task 8 scope and objectives, thereby bridging gaps between applied and fundamental research.

2 Preliminary estimate of resaturation times and impact of key modeling assumptions

The effects of commonly used simplifying assumptions and their impact on unsaturated flow behavior in the bentonite-rock interface are studied using numerical models with 2D representations of the site setting. Also, the impact of fracture properties, in particular the fracture transmissivity and the location of the fracture outlet along the deposition hole are evaluated in terms of re-saturation times and behavior. The analyses presented in this chapter relate to and further extend the problem description of Task 8a of the task definition. More details about the methods and results presented in this chapter can be found in the separate article by Dessirier et al. (2014).

2.1 Objectives

The objectives of the analysis presented in this chapter are

- to provide an estimate of re-saturation times of the bentonite buffer,
- to assess potential transient de-saturation of the rock matrix,
- to evaluate the relative importance of the phenomena and processes in action and identify those which may be of secondary importance or that may be disregarded,
- to establish necessary methodology and modeling strategies, including technical work flow and tools (meshers, fracture network generators, solvers, visualizers, scripting routines).

2.2 Approach

A scenario analysis is carried out where different conceptualizations of unsaturated flow are compared, namely

- simplified unsaturated groundwater flow according to Richards' equation where only liquid water is physically accounted for- and
- two-phase flow theory where both water and air are each subject to a mass balance.

These are the first two cases presented in Table 2-1: eos3 for the full two-phase flow setup and eos9 for the simplified 'setup using Richards' equation.

For this part, the model setup is a radial generic model of a cylindrical rock domain with 20 m radius, and 45 m-height and where a tunnel and a deposition hole are represented on the symmetry axis (Figure 2-1). The tunnel is a 5 m high vault that is 4 m-wide at its base (so 2 m width after symmetry is considered in the present model, see Figure 2-1). The deposition hole is 3 m-high (between its bottom point at $z = 17$ m and the tunnel floor at $z = 20$ m). It has a radius of 0.15 m (See Figure 2-1). A fracture intersects the deposition hole at mid-depth in the base case scenario (at $z = 18.5$ m in Figure 2-1). The problem domain is meshed by a 3D Voronoi tessellation algorithm. With this technique, one starts by defining points of interest which will become the cell centers of the final mesh. Special attention can be given to meshing regions of interest, such as the bentonite buffer and fracture by increasing the density of points inside and nearby. The domain is then partitioned in computational cells according to a nearest neighbor criterion so that each point of interest receives all points in space that are closer to it than any other defined point. The resulting mesh is described in Figure 2-1. This method allows us to refine the mesh around the deposition hole with optimum flexibility while keeping a lower mesh density for regions far from the interface (Figure 2-1).

Table 2-1. List of Scenarios.

Scenario	Description
eos3	Base case, full two-phase flow description as implemented in TOUGH2-EOS3, the fracture hits the deposition hole in its middle (z = 18.5 m).
eos9	The geometry is the same as in the previous case, but two-phase flow is approximated by Richards' equation as implemented in TOUGH2-EOS9.
eos3_up	Same as base case, but with the fracture hitting the deposition hole at its top (z = 19.25 m).
eos3_down	Same as base case, but with the fracture hitting the deposition hole at its bottom (z = 17.75 m).

Numerical modeling is conducted with TOUGH2 (Pruess et al. 1999). Two equation-of-state modules of the TOUGH2 code are used:

- One including full air/water two-phase dynamics (base case eos3 in Table 2-1). Processes in this case include liquid and gas phase advection and possible degassing or gas dissolution.
- One using the common Richards' assumptions that neglects the air mass balance and simply solves the liquid moisture transport (case eos9 in Table 2-1).

Another aspect of the scenario analysis is to examine potential effects of the location of the fracture intersection in the deposition hole. The influence of the fracture transmissivity has not been formally analyzed at this point. Together with the base case eos3, two alternative cases with full two-phase description investigate the changes introduced by moving the horizontal rock fracture up at a quarter of its depth, closer to the tunnel floor (case eos3_up in Table 2-1) or down at three quarter of its depth, closer to the bottom of the deposition hole (case eos3_down in Table 2-1). Together with the base case eos3, they can provide information on how sensitive the predictions are to a rigorous mapping of the fracture intersections with the deposition hole.

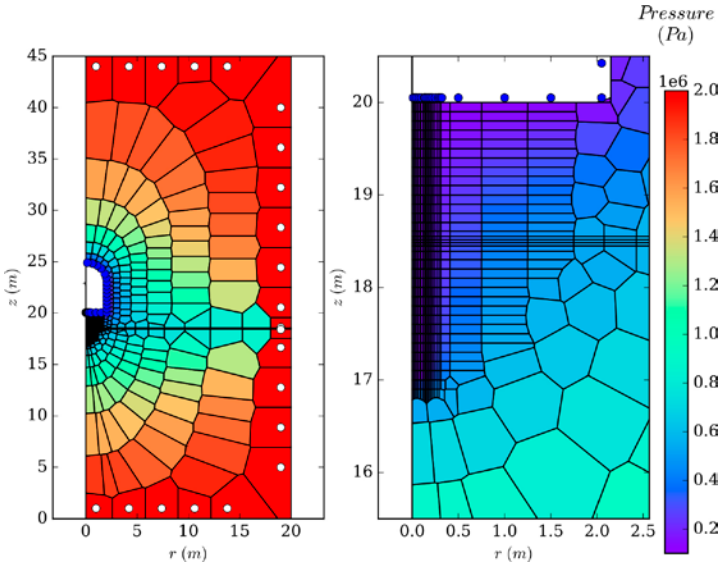

Figure 2-1. *Finite volume radial mesh created by Voronoi tessellation, and Pressure field used as initial condition in scenarios eos3 and eos9 (Table 2-1). Each polygon is a Voronoi cell that defines an elementary volume for the numerical resolution of multiphase flow equations by TOUGH2. A dot in- or outside a cell denotes fixed boundary conditions. The symmetry axis is defined by r = 0, the tunnel is visible in the centre. A close-up view is given on the right. The deposition hole is 3 meters deep from the tunnel floor and has a radius r = 0.15 m. The rock fracture is horizontal at z = 18.5 m and is implemented as 10 cm-thick vein with higher permeability and porosity.*

2.3 Model Setup

Characteristic curves and parameter values for bentonite, rock matrix and rock fracture are taken from the Task 8a definition (Vidstrand et al. 2017). Mechanical effects such as swelling of the bentonite are not addressed directly but taken as alterations of the characteristic curves. Adapted parameters are chosen that reflect confined conditions, see Dueck and Börgesson (2007) for more information.

Boundary conditions are taken as constant pressure (2 MPa on the outer rock domain, atmospheric in the tunnel, see Figure 2-1). Initial conditions are generated by running the model to steady state with the deposition hole left empty using Richards' equation since no air bubbles or entrapment is expected to intervene for a developed steady state prior to the tests. The initial conditions are thus rigorously identical between scenario eos3 and eos9, and they are translated into eos3 variables using the documented properties of water and steam as well as the chosen characteristic curves for the materials used in this application.

2.4 Results

Simulation results are presented in terms of transient liquid pressure (Figure 2-2 and Figure 2-3) and liquid saturation fields (Figure 2-4 and Figure 2-5) close to the deposition hole for selected snapshots in time ranging from t = 1 hour (leftmost panel), to t = 1 day (second-left panel) to t = 1 year and beyond (right panels) for simulation scenarios eos3 and eos9.

The transient saturation development for the two adjacent cells across the bentonite rock/interface at the fracture depth (z = 18.5 m, Red curves) and at three quarter depth of the deposition hole (z = 17.75 m, blue curves) is also provided as Figure 2-6. Solid lines show the saturation profile on the side of the bentonite (r = 0.14 m) while dashed lines show the pressure on the rock-fracture or rock-matrix side (r = 0.16 m).

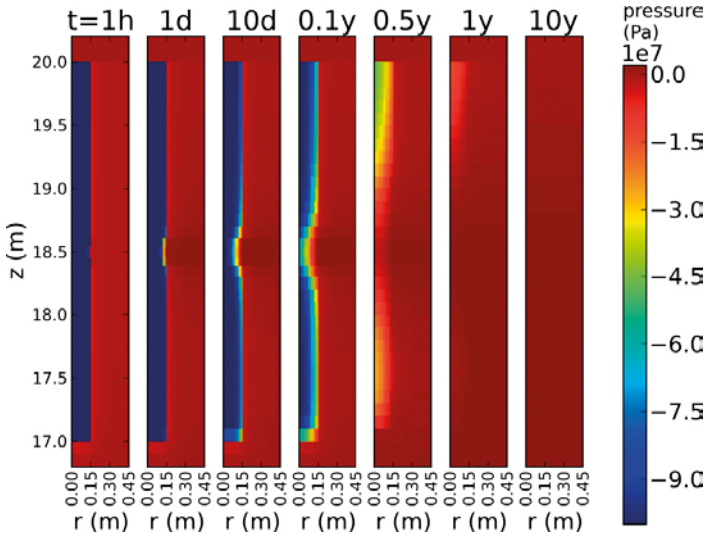

Figure 2-2. *Liquid-phase pressure profile close to the deposition hole under scenario eos3 (Table 2-1). The deposition hole is 3 meters deep from the tunnel floor and has a radius r = 0.15 m. The rock fracture is horizontal at z = 18.5 m. The maximum positive pressure is 2 MPa at the distant exterior boundary condition (not visible on this picture) and 1atm on the tunnel floor here at z = 20 m. Negative pressures in the deposition hole (r < 0.15 m) and the nearby rock domain denote unsaturated conditions. The initial suction in the installed bentonite is 100 MPa.*

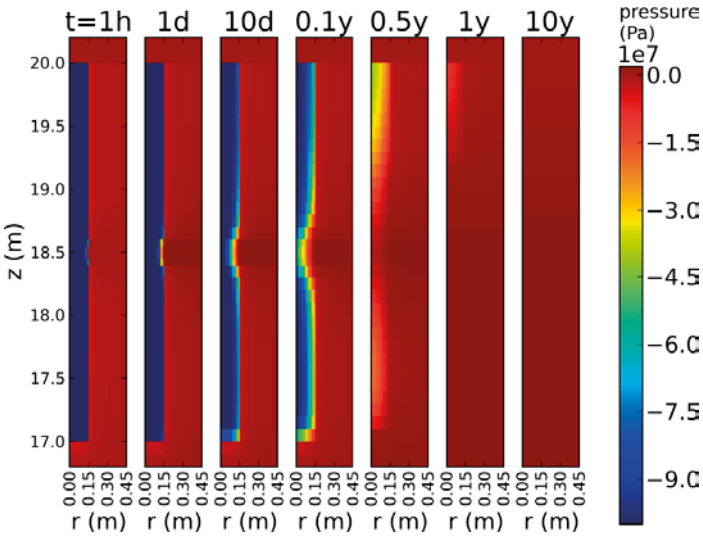

Figure 2-3. *Liquid-phase pressure profile close to the deposition hole under scenario eos9.*

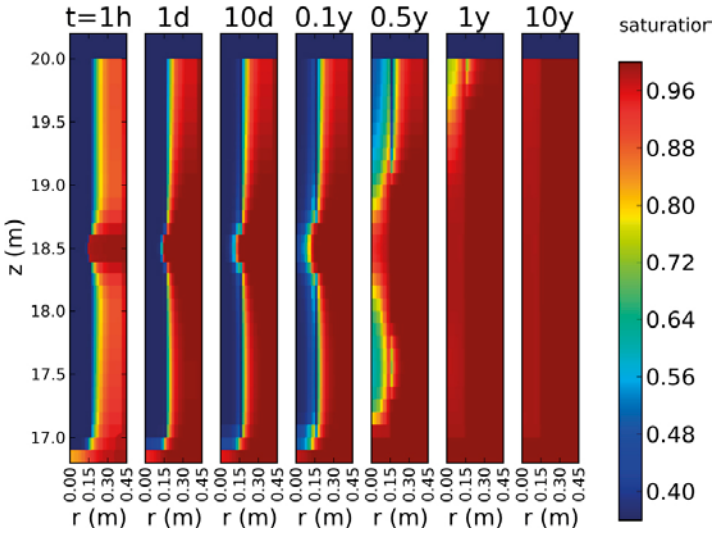

Figure 2-4. *Liquid saturation profile near the deposition hole under scenario eos3 (Table 2-1). The deposition hole is 3 meters deep from the tunnel floor and has a radius r = 0.15 m. The rock fracture is horizontal at z = 18.5 m. The initial saturation is 0.36 in the bentonite and 1.0 in the rock domain. One can clearly notice a de-saturation of the rock matrix (r > 0.15 m) for an extended period of time. The same phenomenon occurs for the rock fracture but is resaturated within the first hour of the experiment.*

After the deposition hole is filled with bentonite at t = 0, pressure starts to increase in the rock domain and in the fracture as the bentonite gets wetted to eventually reach positive values, numerically close to the applied 2 MPa on the outer boundary. The pressure response is very similar for the case with air constituent (eos3, Figure 2-2) compared to the case with Richards approximation (eos9, Figure 2-3). Neither with a wide pressure scale including negative values presented here (Figure 2-2 and Figure 2-3), nor on a narrower scale focused on positive values for the saturated zone (not shown here) does one observe any noticeable difference.

Saturation increases in the bentonite buffer after installation at t = 0. A general observation for all scenarios is that the re-saturation times in different regions of the bentonite buffer can be categorized according to the following (from shorter to longer): (i) close to the fracture, (ii) below the fracture intersection, and (iii) above the fracture intersection. We can identify an influence of the tunnel in the upper part. In all considered scenarios (Table 2-1), re-saturation is faster close to the fracture-deposition hole intersection at z = 18.5 m (Figure 2-6; bold red curves) than further away from it (Figure 2-6; thin blue curves), by about 3 orders of magnitude.

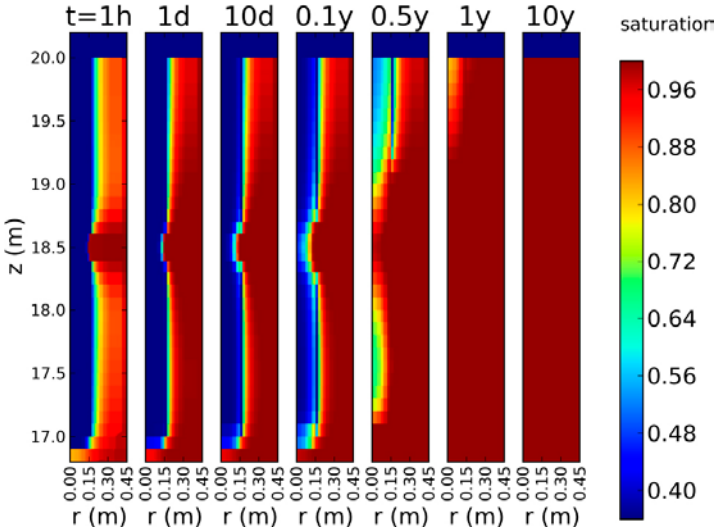

Figure 2-5. *Liquid saturation profile near the deposition hole under scenario eos9 (Table 2-1).*

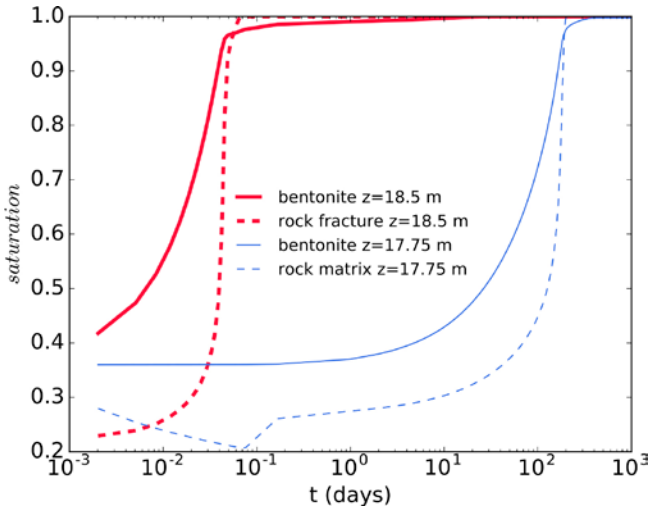

Figure 2-6. *Liquid saturation at the bentonite/rock interface at two different depths for scenario eos3. Solid lines give saturation in the outermost layer of bentonite (r = 0.14 m) and dash lines correspond to saturation in the rock domain just outside of the deposition hole (r = 0.16 m). The red curves show the saturation at the fracture depth (z = 18.5 m), and the blue curves show the saturation below the fracture (z = 17.75 m), where the bentonite is in contact with the homogeneous rock matrix.*

Comparing the water saturation levels given by simulation scenarios eos9 and eos3 at any given simulation time (Figure 2-4 and Figure 2-5), up to 9 % saturation difference could be observed in the considered domain at some distance from the tunnel, however with values up to 30 % immediately under the tunnel floor. Richards' equation systematically gives higher values of water saturation. The difference between the predictions increases with time until eos9 reaches full saturation, at which point the gap starts to decrease, as it can be expected.

The initial water saturation degree is 0.36 in the bentonite and 1.0 in the rock. However, the installation of bentonite in the deposition hole at t = 0 rapidly induces a long-lasting de-saturation of the closest region of the rock domain. Notably, the saturation degrees in the rock (Figure 2-6; dashed curves) become lower than in the bentonite itself (Figure 2-6; solid curves). This is a consequence of a high suction of the unsaturated bentonite, which when transferred to the rock domain causes a relatively large de-saturation. This effect seen in the present results (Figure 2-6), suggests that it can be relevant to further investigate such dynamics by use of refined models, e.g. accounting for effects of non-darcian flows in dual-porosity models (Liu et al. 2012, Åkesson and Kristensson 2008) and/or mechanical effects on the retention curve (Rutqvist et al. 2011, Åkesson and Kristensson 2008).

Furthermore, it can be seen in Figure 2-4 and Figure 2-5 that the unsaturated zone developed under the fracture plane in the rock matrix (at z ~ 17.75 m) between 0.1 year and 0.5 years (at which point some rock cells still display up to 30 % gas saturation) is predicted to have a longer residence time when full two-phase flow dynamics are considered. This illustrates a risk for some degree of air entrapment that a traditional modeling approach using Richards' equation is not empowered to predict, and it indicates that an appropriate description of degassing/dissolution mechanisms is required to eliminate uncertainties related to possible air trapping.

Another way to analyze the results is to isolate the time t_α it takes for a particular cell to reach and stay above a certain percentage of saturation α. Figure 2-7 and Figure 2-8 show the spatial distributions for t_{50}, t_{90}, t_{95}, t_{98} and t_{99} under both scenario eos3 and eos9. Figure 2-9 and Figure 2-10 show in more details the comparison of re-saturation times between the two scenarios eos3 and eos9 at specific depths in the model, namely in the fracture plane (z = 18.5 m) and at some distance below it (z = 17.75 m) as a function of the radial coordinate r.

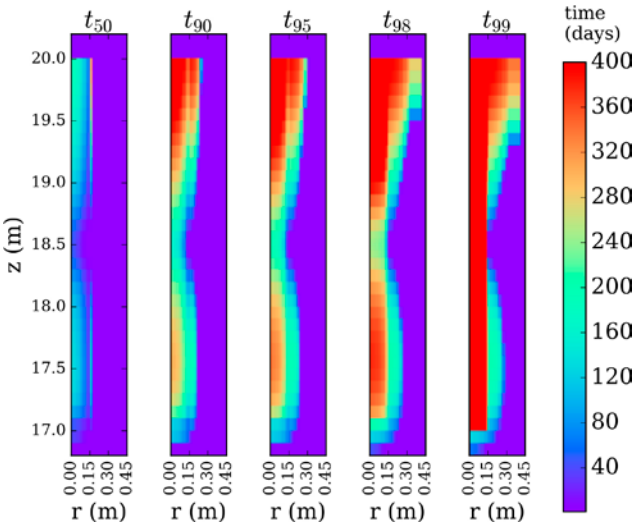

Figure 2-7. *Times to reach defined percentages of saturation under scenario eos3 (Table 2-1). The deposition hole is 3 meters deep from the tunnel floor and has a radius r = 0.15 m. The rock fracture is horizontal at z = 18.5 m. The total simulation time was 1 000 days at which point cells in the buffer had still not reached 99 % saturation. This justifies the choice of the maximum value in the scale to illustrate better the differences at lower saturation degrees.*

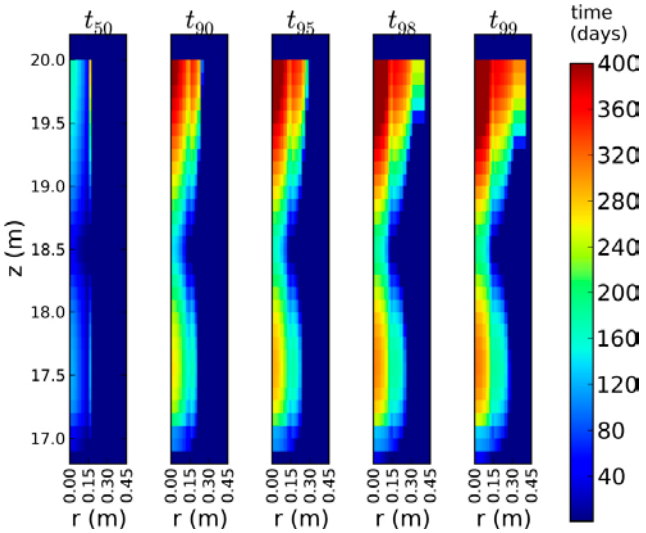

Figure 2-8. *Time to reach defined percentages of saturation under scenario eos9 (Table 2-1).*

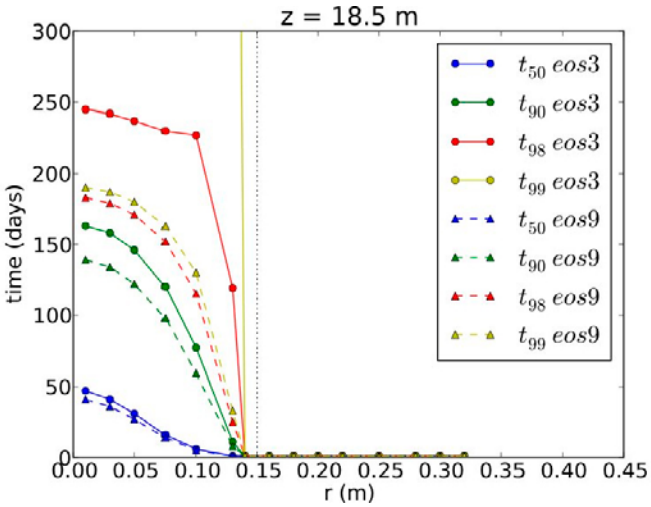

Figure 2-9. *Times $t_\alpha(r)$ required to reach different fractions of saturation α in the fracture plane (z = 18.5 m) under scenario eos3, as a function of the radius r. The symbols represent finite volume centers in the modeling; the provided lines are only linear interpolations between those points.*

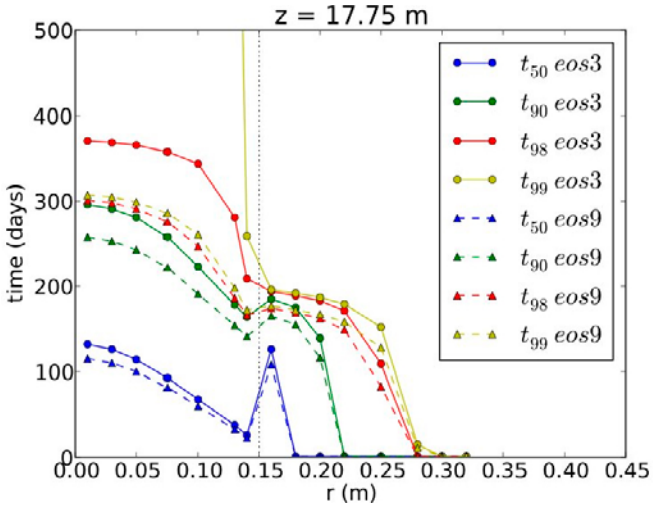

Figure 2-10. *Times $t_\alpha(r)$ required to reach different fractions of saturation α below the fracture plane (z = 17.75 m) under scenario eos3, as a function of the radius r. The symbols represent finite volume centers in the modeling; the provided lines are only linear interpolations between those points.*

Table 2-2 gives times needed for all parts of the bottom three quarters of the bentonite buffer to reach certain degrees of saturation for all tested scenarios. The upper part is not included in order to avoid a strong influence of the zone disturbed by the presence of the tunnel on the presented re-saturation times. Only the minimum saturation in the lower region of the buffer is tracked, no consideration is given to the average value. The relative deviation from the base case eos3 is given as a percentage.

Table 2-2. Times (in days) needed to reach different percentages of saturation in all cells in the lower three quarters of the inserted buffer. The difference relative to the base case is given in parenthesis.

Days	t_{50}	t_{90}	t_{95}	t_{98}	t_{99}
eos3	170	344	389	488	>1 000
eos9	156 (−11.2 %)	302 (−12.2 %)	335 (−13.9 %)	362 (−25.8 %)	373
eos3_up	193 (+13.5 %)	356 (+3.5 %)	391 (+0.5 %)	436 (−10.6 %)	>1 000
eos3_down	302 (+77.6 %)	461 (+34.0 %)	510 (+31.1 %)	691 (+41.7 %)	>1 000

As already seen with the saturation profiles, saturation times are shorter respectively: across the fracture intersection, then below the fracture plane, and finally longer close to the tunnel floor. In the base case eos3, which accounts for both air and water mass conservation, the simulated time to reach 95 % saturation in the zone of interest in the deposition hole is approximately 389 days (Table 2-2). The simplified flow description eos9, which neglects air mass conservation, gives lower estimates of re-saturations times (e.g. 335 days for 95 % saturation). Investigating how two-phase flow dynamics can influence re-saturation times, one can see that there is a systematic difference here as well.

However, whereas the difference in saturation values prescribed by the two scenarios remained close to 9 % difference in degree of saturation, regarding estimated times to reach a certain fraction of saturation (Table 2-2, Figure 2-7 and Figure 2-8), the higher the considered saturation fraction, the greater the two predictions diverge. The disagreement increases as full saturation is approached (Figure 2-9 and Figure 2-10) to the point that it could not be estimated within the simulated time frame (1 000 days) for t_{99} in the two-phase case eos3 (Figure 2-7). Scenario eos9 reaches explicitly full saturation in less than 400 days (Figure 2-8) but scenario eos3 never overreaches 99 % in the bentonite. Consequently, the relative difference in re-saturation times jumps from 14 % for 95 % saturation, to 25 % for 98 % saturation to more than 60 % for 99 % saturation (Table 2-2).

This implies that a full consideration of two-phase flow dynamics may in particular be needed for estimating times to reach full (or near-full) water saturations, since the use of Richards' equation may lead to significant underestimations under such conditions. Furthermore, the difference in estimated saturation times is also globally an increasing function of the distance to the source of water (Figure 2-9 and Figure 2-10). In the present configuration, the smaller the radial distance r from the center of the deposition hole (i.e. further away from the saturated zone), the higher the disagreement between the two predictions. A thicker buffer layer might then face even larger prediction errors.

Investigating effects of fracture position on re-saturation times (scenarios eos3, eos3_up and eos3_down of Table 2-2), one can see that impacts can be considerable, with differences up to 78 % in the investigated cases. So it is obvious that the rock fracture network has a strong influence on the re-saturation profiles and times but the observation made under scenario eos3 regarding which regions of the model relative to the fracture position are subject to faster re-saturation remain true. The global time scales for re-saturation are more meaningful than the detailed profiles themselves in which the same patterns as those observed for scenario eos3 would be apparent but re-centered on the fracture level. That is why the full profiles of pressure, saturation and re-saturation times are not shown here and only the global time scales of those experiments are reported in Table 2-2. Overall, the maximum time to reach 98 % stayed under 2 years (Table 2-2) for the tested fracture positions.

Up to 95 % saturation, the configuration with shortest re-saturation times is the one for which the flow paths from the fracture outlet to any point in the deposition hole is the shortest, i.e. the eos3 configuration with the fracture in the middle. However, the shortest time to reach higher saturations (98 %) is obtained for the configuration with the fracture at the top, i.e. the eos3_up configuration, showing that the fracture position becomes less significant for the global behavior of the deposition hole as steady-state conditions approach, meaningful factor to estimate full saturation is the hydraulic gradient seen at the fracture outlet, so between the fracture and the tunnel. The presence of excavations and the conditions imposed at the tunnel wall seem to dominate at the latest stages.

Figure 2-9 and Figure 2-10 show re-saturation times for the case that the envisioned fracture intersects the middle part of the deposition hole. The shown profiles of times required to reach a certain saturation level α at a certain radial distance r, i.e. $t_\alpha(r)$, are not altered by the fracture position. The shape of t_{98} at the fracture depth in eos3_up or eos3_down is consistent with the one obtained at $z = 18.5$ m for eos3 (Figure 2-9), and the shape of t_{99} away from the fracture is similar to the ones shown for other depths in Figure 2-10, however the vertical time scale varies, so that the absolute times concur with the values given in Table 2-2.

2.5 Discussion, fate of the air component

This section contains an analysis of the fate of the air present in the pores of bentonite and the host rock.

The liquid relative permeability of the bentonite was described by a power law: $k_{r,liq} = S_{liq}^3$. This approach has been pointed out as relevant in several experimental determinations. The sensitivity to the value of the power law exponent was not tested here. However, two different assumptions were tested regarding the relative permeability of the gas phase: one with more restricted gas flow, where $k_{r,gas} = (1-S_{liq})^3$, and another allowing more gas mobility, where $k_{r,gas} = 1$. The results are shown in Figure 2-11 by the set of black and green curves respectively. The simulation could not be carried out for as long time as the previously described case due to extensive computational times.

The high porosity of bentonite compared to the host rock causes the air mass hosted by the rock (not shown in Figure 2-11) to be negligible in comparison to that in the bentonite. Therefore, the air dissolved in bentonite water (dashed lines) and the air that exists as a separate gas phase in the bentonite (dash-dotted lines) practically add up to the total amount of air in the system (solid lines).

The solid black line shows that, under a restricted gas relative permeability, virtually no air exits the system through the tunnel. Instead, air goes into solution (see the increasing trend of the dashed line) and remains in the system for long times. Simulation results for $t > 1\,000$ days are presently not available due to the associated long simulation times. However, if the slow decrease of the solid line is extrapolated, it would give a removal time of air on the order of several thousand years.

Figure 2-12 shows the air repartitioning and dissolution in the water of the system. In the beginning ($t = 1$h), there is only very low amounts of air dissolved in water. This is because pressures are still low (Figure 2-2) such that air exists mainly as a separate gas phase (yielding low water saturations; Figure 2-4). Dissolution starts first at spots of high pressure, for instance at the fracture outlet into the deposition hole and at the bottom of the deposition hole further away from the tunnel. This is directly in line with the used Henry's law assumption that the gas solubility is proportional to the gas partial pressure and that the dissolution process reaches equilibrium much faster than the advective flow does. It can therefore be considered to be instantaneous. One can also notice that with no molecular diffusion accounted for, virtually no dissolved air migrates from the bentonite to the neighboring rock matrix, which, once the rock matrix is resaturated as observed, is consistent with a driving groundwater flow occurring from the rock matrix to the bentonite.

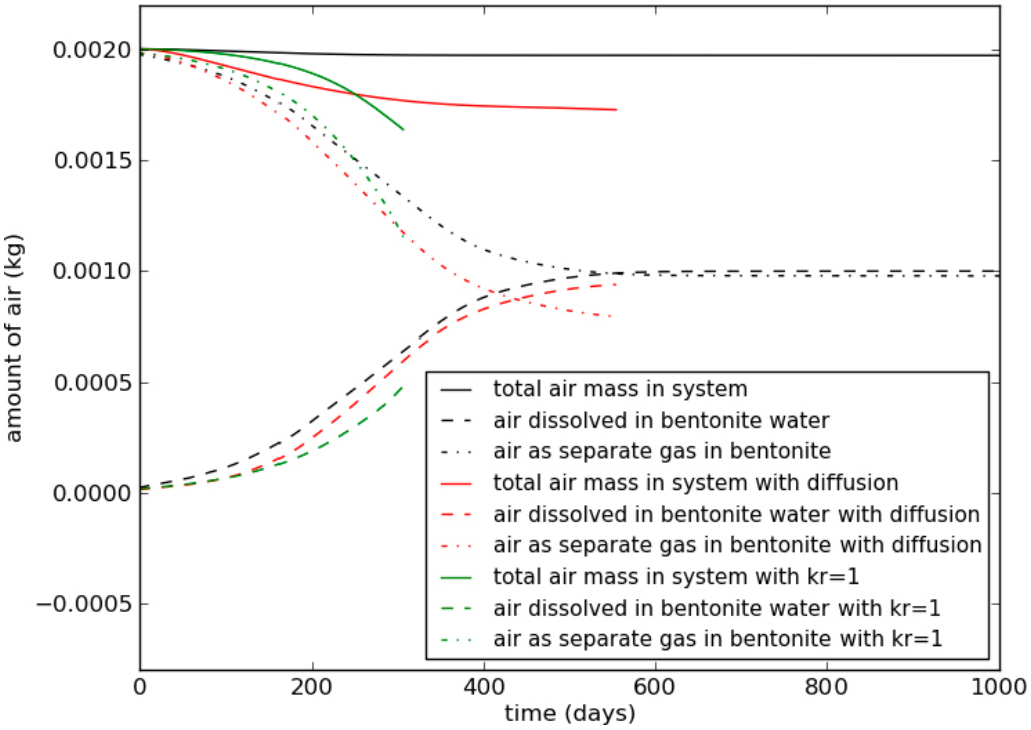

Figure 2-11. *Evolution and partition of air in the model (scenario eos3, in black and eos3 with molecular diffusion, in red, and with a more permissive gas permeability, in green).*

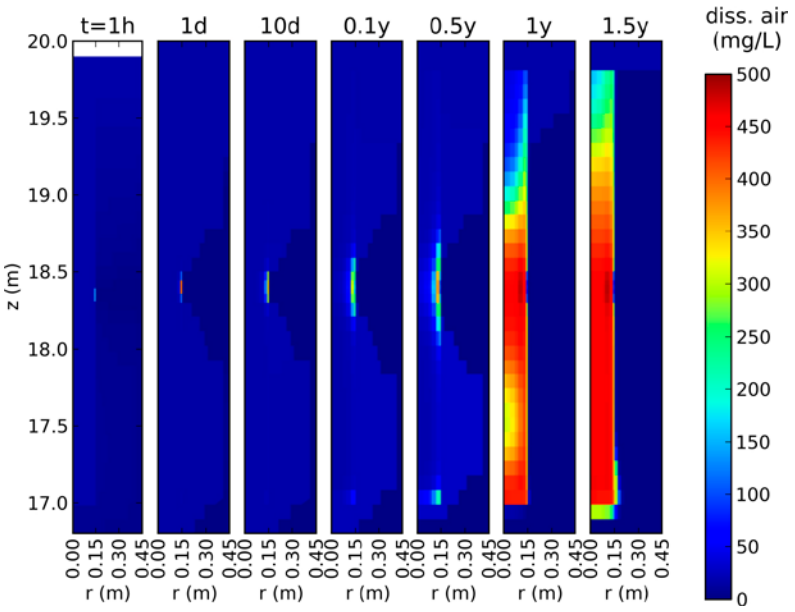

Figure 2-12. *Predicted concentration of air dissolved in water, without consideration of diffusion. The deposition hole is 3 meters deep from the tunnel floor and has a radius r = 0.15 m. The rock fracture is horizontal at z = 18.5 m.*

Assuming a more permissive relative permeability (green) air is removed much quicker through outflow in the tunnel. Yet about ¾ of the initial mass of air is still present in the system after one year, which is when the bentonite has approximately reached 95 % saturation (Figure 2-4). The corresponding removal time is on the order of a couple of years.

Considering that advective water and air transport can become very slow in bentonite, the influence of a diffusion process of dissolved air in the liquid phase was also tested. The set of red curves in Figure 2-11 show the results for the restricted gas permeability scenario, with molecular diffusion turned on. One can notice a tangible decrease compared with the case with no diffusion (black set of curves). The typical extrapolated removal time for air would in this case be around several decades. Figure 2-13 shows the evolution and repartition of dissolved air with molecular diffusion. Compared with Figure 2-12, one can remark that molecular diffusion irons out the occurrence of the first spot where dissolved gas starts to appear. Another observation is that with the diffusivity value that was tested, dissolved air is now able to migrate into the rock matrix, and the displayed example shows a penetration of approximately 10 cm within the first year and a half (Figure 2-13, right panel). One would then have to estimate the uncertainty on the considered diffusion coefficients for diffusion of air in free water ($D_m = 2 \times 10^{-9}$ m^2/s) and the scheme to adapt this diffusion to an equivalent porous medium here assumed to be represented by a tortuosity $\tau = \Phi^{1/3} S_l^{10/3}$ (Φ being the porosity and S_l the liquid saturation) in accordance with the model introduced by Millington and Quirk (1961) and implemented in TOUGH2 (Pruess et al. 1999, Appendix D, p 156).

In addition to the uncertainties on the physical processes, some reactive components of air such as oxygen could undergo different biogeochemical transformations, dramatically changing residence times. Yang et al. (2007) showed that depending on which set of biogeochemical reactions are considered, the time needed to consume the initially dissolved oxygen in the bentonite buffer can range from 5 000 years to 19 days.

To relate the latter study with the present study, one can compare the here predicted dissolved air/oxygen concentrations (Figure 2-12 and Figure 2-13) with the corresponding initial assumptions made by Yang et al. By assuming an initial partitioning of air similar to the atmospheric ratio (23 % O_2 by mass), the here used model suggests values around 3.5 10^{-3} mol O_2/L which is about 10 times higher than the initial values reported by Yang et al. In light of the present study, greater dissolved oxygen amounts could potentially feed microbial ecosystem growth and consequently impact corrosion risk.

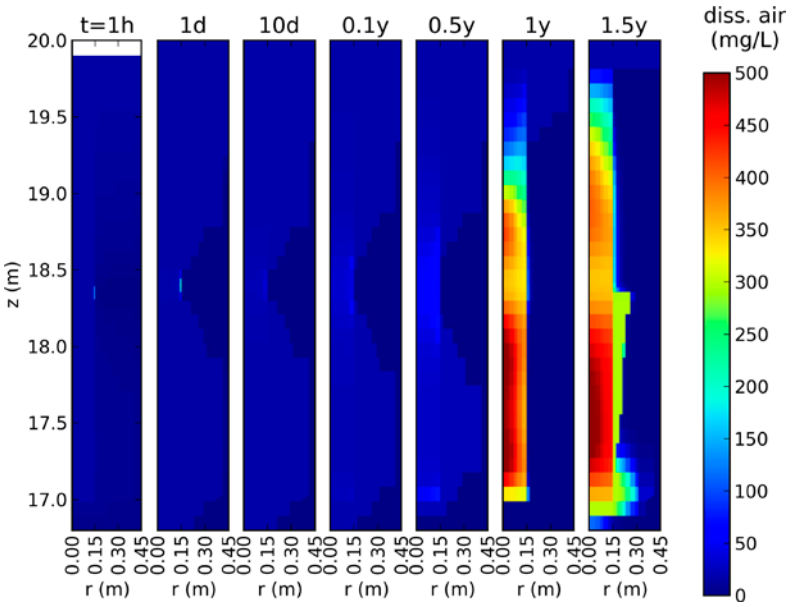

Figure 2-13. *Predicted concentration of air dissolved in water, with air diffusion in the liquid.*

Some studies (see Alonso et al. 2005) showed greater gas mobility and questioned the concept of intrinsic permeability at low water saturation degrees (typically under 60–70 %) for expansive materials like bentonite due to the swelling effect. They proposed gas permeabilities in this range up to two orders of magnitude higher than the traditionally defined intrinsic permeability. In comparison to the results discussed in this report, this could mean that air could leave the system almost freely and without gas pressure increase from $S_{g,initial} = 0.64$ until the swelling occurs and the gas permeability drops to a level comparable to that of the liquid (estimated at $S_g \sim 0.3$), such that the dissolution process observed would apply to a reduced amount of about $(0.64 - 0.3) \times 100 \sim 30$ % of the original air mass present in the bentonite pore space. It is too early to draw definite conclusions, but the concept of intrinsic permeability should be tested in this context. The uncertainties related to the residence times of the air can be listed as follows:

- Incorporation of biological and geochemical processes.
- Possible questioning of the concept of intrinsic permeability for bentonite.
- Parametrization of the decrease in gas relative permeability at high saturations.
- Parametrization of the molecular diffusion of dissolved air in groundwater.

2.6 Conclusions and Recommendations

This study demonstrates that, with state-of-the-art parameterizations of hydrological properties of engineered bentonite and investigated rock types, the installation of a bentonite buffer can cause considerable de-saturation of the adjacent rock matrix. This can influence the environment near the deposition holes as well as the physical and biogeochemical processes along the transport pathways from the repository. Furthermore, the relatively large de-saturation effect seen in the present results, later corroborated by humidity measurements on rock samples from the dismantled BRIE deposition hole walls, suggests that it can be relevant to further investigate such dynamics by use of refined dual-porosity and/or mechanical models to correctly describe the bentonite/rock interface.

Preliminary estimates of the re-saturation times indicate that 95 % saturation will be reached within two years for most of the installed buffer. Investigating effects of fracture position on re-saturation times (to 95 %), one can see that impacts can be considerable, with differences up to 78 % in the investigated cases.

A comparison between full two-phase flow modeling and simplified unsaturated flow modeling with Richards' equations showed that Richards' equation systematically predicts higher degrees of liquid saturation and shorter re-saturation times than the model with full two-phase flow representation. This difference is relatively small (10–15 %) at lower water saturations. Since the required calculation (model-run) times were found to differ by more than one order of magnitude, Richards' equation is expected to be useful in cases (e.g. for lower saturations) where bubble entrapment and gas dissolution can knowingly be neglected. Notably, the difference between the models increases as the system approaches saturation, which implies that Richards' equation may lead to significant underestimations of times to reach full (or near-full) water saturations. For instance, the considered simulation time of 1 000 days was too short to reach 99 % saturation with the full two-phase flow representation, whereas 99 % saturation was predicted to be reached in 373 days using Richards' equation. Hence, attention should be paid to detailed modeling of two-phase flow dynamics in the near-canister domain, e.g. characterizing unsaturated flows at the points of intersection of the deposition holes with the surrounding fracture network, when such considerations are relevant. However, the implementation of two-phase flow dynamics is computationally demanding so that its use may need to be restricted to a limited radius where degassing/dissolution is likely to be most significant.

A more open and fundamental question is the ultimate fate of the air included in the bentonite at installation. Exploratory scenarios laid out here showed that a main part of the air could in fact undergo dissolution instead of migrating out of the deposition hole as a separate gas phase. This possibility implies in principle that biogeochemical processes could be triggered and become important for the performance of the repository.

3 Global sensitivity analysis of buffer near-saturation time, rock wall re-saturation time and dissolved air in bentonite pore water

3.1 Objective

Following the scoping calculations presented in the previous chapter, a new analysis was set up to systematically establish ranges for three predictions of interest: (i) the predicted saturation time in the buffer, (ii) re-saturation time of the rock wall and (iii) the amount of air initially introduced with the buffer that undergoes dissolution into the liquid phase, and this, given a wide set of conditions regarded as representative of those observed in the BRIE tunnel or potentially of a KBS-3 deposition hole.

3.2 Approach

This chapter present a semi-quantitative global sensitivity analysis of some model outputs (or predictions, for example time to reach 95 % saturation) to an array of model inputs (or parameters, such as local intrinsic matrix permeability or intersecting fracture transmissivity).

The results summarized in this chapter were published as a separate article (see Dessirier et al. 2015).

For this global sensitivity analysis, the framework of the elementary effects introduced by Morris (1991) was adopted as extended by Campolongo et al. (2007). Eleven input parameters (Table 3-1) were selected with estimated bounds to build an input parameter space. The parameters were assumed independent, uniformly distributed between their respective bounds and each dimension was discretized with a finite level of possible values (here four). The method of Morris defines the elementary effects EE_i for an output y with regard to an input X_i (all other inputs remaining unchanged) as $EE_i = [y(X_i+\Delta) - y(X_i)]/\Delta$ where Δ is a transition between two discrete levels in the dimension corresponding to parameter X_i. Sampling the EE_i for each parameter X_i over the hyperplane orthogonal to it and for different start levels along the dimension of X_i allows to assess the sensitivity of this particular output y to each input parameter by analyzing the statistics $\mu^* = \text{mean}(|EE_i|)$ and $\sigma = \text{std}(EE_i)$. To reduce the cost of the global evaluation scheme, Morris defined trajectories as sequences of points in the input parameter space obtained by successive one-dimensional jumps. Each points along a trajectory can then be involved in the calculation of two elementary effects (except the start and end point of the trajectory). The starting points are distributed randomly. Campolongo et al. (2007) proposed a distance between trajectories in order to define and maximize the spread of the set of random trajectories used to compute the elementary effects. For this analysis, each of the eleven dimensions were discretized with 4 levels and the 10 trajectories with the highest spread out of 500 were used, which led to $(11+1) \times 10 = 120$ parallel simulations. The implementation of Morris' method in the open-source package SALib was used for this study.

3.3 Model setup

A simple 2D radial mesh, similar to the mesh used in the previous chapter, was used to limit the computational effort and to easily parametrize the position of the intersecting fracture as one of the input parameters (see Table 3-1 and Figure 3-1). Other input parameters tested for sensitivity were hydraulic parameters of the rock mass near the deposition hole: fracture transmissivity and specific storage (porosity), rock matrix intrinsic permeability and porosity. The air entry pressure was assumed to be correlated to the intrinsic permeability both in the fracture and the rock matrix and thus scaled by the inverse of the square root of the transmissivity or permeability (Leverett 1941). Three parameters described the relative permeabilities in the bentonite: two exponents and an absolute difference between gas-saturated and liquid-saturated permeabilities as reported by Alonso et al. (2005) for FEBEX bentonite, and implemented here as a custom TOUGH2 relative permeability relation. Additional

parameters were the equivalent suction exerted at the tunnel boundary due to evaporation and ventilation, the far field water pressure in the rock (as a reflection of the depth of the tunnel or possible drawdown created by neighboring cavities) and finally the diffusivity of dissolved air in liquid water.

All simulation setups and runs were handled using the PyTOUGH library (Croucher 2011). Several outputs (predictions) were analyzed and are now presented as separate sections.

Table 3-1. sensitivity analysis parameters.

Parameter	Unit	Symbol	Min	Max	Reference
Fracture position	[m]	z_f	–2.75	–0.25	–
Rock saturated permeability	[$\log_{10}$ m^2]	$\lg K_r$	–20	–18	Fransson et al. (2017)
Rock porosity	[$\log_{10}$–]	$\lg \Phi_r$	–5	–3	Fransson et al. (2017)
Tunnel suction	[Pa]	p_c^{tunnel}	10^5	5×10^7	Finsterle and Pruess (1995)
Fracture transmissivity	[$\log_{10}$ m^3]	$\lg T_f$	–10	–8	Fransson et al. (2017)
Fracture porosity	[$\log_{10}$–]	$\lg \Phi_f$	–4	–2	–
Bentonite liquid permeability exponent	[–]	α	2	5	Fransson et al. (2017)
Bentonite gas permeability exponent	[–]	β	2	5	Fransson et al. (2017)
Ratio between gas-saturated and liquid-saturated permeability in bentonite	[$\log_{10}$–]	$\lg \Gamma$	2	8	Alonso et al. (2005)
Outer pressure	[Pa]	P_{bnd}	10^6	5×10^6	Svensson et al. (2008)
Air diffusion coefficient	[$\log_{10}$ m^2/s]	D_m	–10	–8	Cussler (1997)

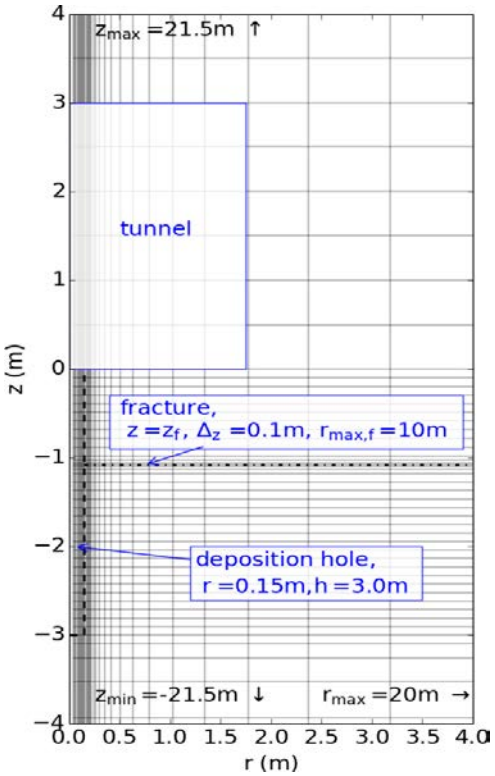

Figure 3-1. *2D radial geometry and mesh used for the global sensitivity analysis. The fracture position depends on the simulation and is re-meshed accordingly.*

3.4 Time to 95 % saturation in the bentonite

The main prediction of interest is the time required to nearly saturate (saturation above 95 %) the buffer. Figure 3-2 and Figure 3-3 show the cumulative density function (CDF) and sensitivity measures of the time required to nearly saturate 25 % of the whole buffer, 50 % of the whole buffer and 75 % of the whole buffer respectively. The empirical cumulative density function (CDF) in Figure 3-2-top for example, shows that the time needed to nearly saturate ¼ of the installed buffer ranges approximately from 11 to 7 000 days with a median around 200 days. The statistics of the elementary effects are represented by the points in the (μ^*,σ) plane and their associated uncertainty bars corresponding to a confidence level of 95 % estimated by re-sampling. The parameter with highest sensitivity are found to the top right of the figures (simultaneous high values of μ^* and σ), in the case of Figure 3-2-top and in decreasing order, the permeability of the rock matrix lgK_r, the outer boundary pressure, the ventilation induced suction at the tunnel wall p_c^{tunnel} and the position of the fracture z_f.

One can actually remark that these four parameters are consistently inducing the highest sensitivity in both Figure 3-2 and Figure 3-3. Also, the closer to global saturation of the buffer one gets, the more these parameters become dominant relatively to the other parameters. To qualify a parameter as having a negligible influence on the tested outputs, one would for example show that its elementary effects moments μ^* and σ are much lower than the range of responses obtained for that output. Following this criterion, one can see that no parameter can strictly be regarded as negligible for the prediction of nearly saturating ¼ of the deposition hole, two parameters can be considered negligible for saturating ½ of the deposition hole, and four parameters can be discarded for ¾ of the deposition hole. The largest uncertainty bars obtained by re-sampling point to parameters involved in interactions with other parameters or causing strongly non-linear responses. These different observations indicate that the saturation time of the buffer is a prediction with a complex sensitivity structure due to a high number of influential parameter with non-linearities and/or parameter interactions.

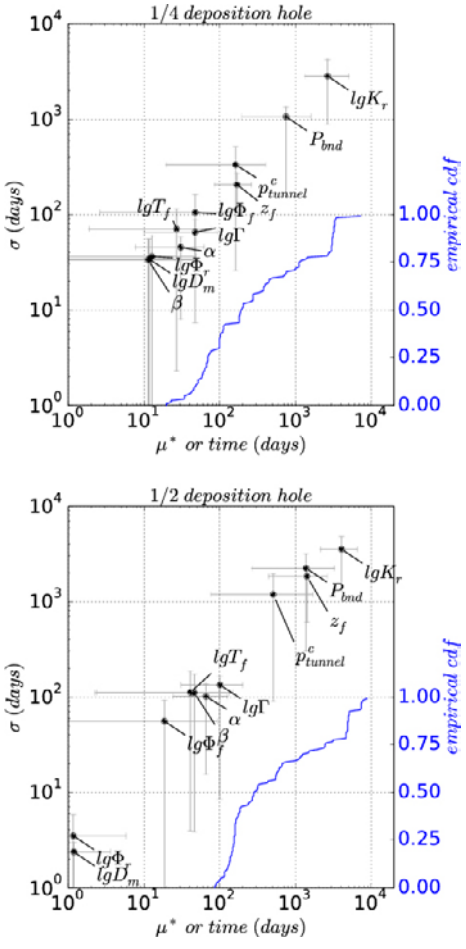

Figure 3-2. *Empirical Cumulative Density Function (blue) and Elementary effect distribution in the (μ^*,σ) plane for the time to nearly saturate 1/4 of the inserted buffer (top) and 1/2 of the installed buffer (bottom).*

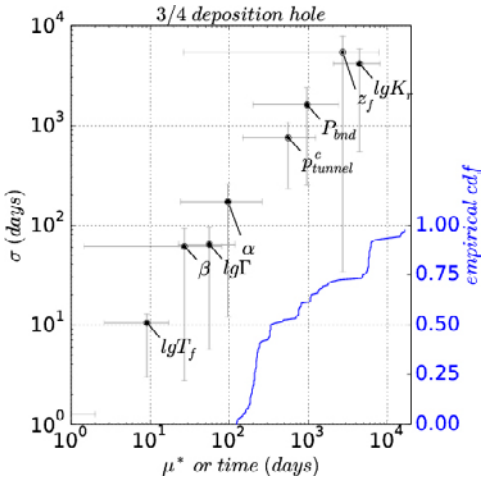

Figure 3-3. *Empirical Cumulative Density Function (blue) and Elementary effect distribution in the (μ*,σ) plane for the time to nearly saturate 3/4 of the inserted buffer.*

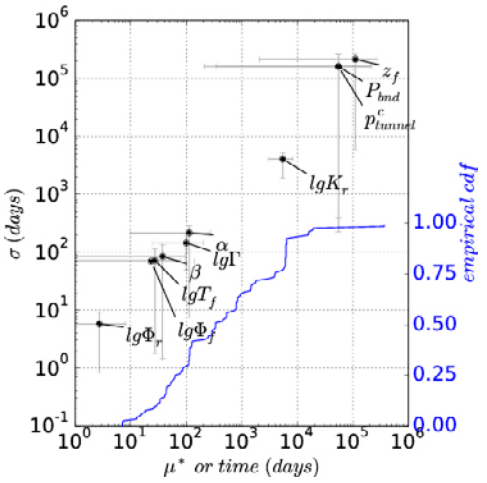

Figure 3-4. *Empirical Cumulative Density Function (blue) and Elementary effect distribution in the (μ*,σ) plane for the time to re-saturate the rock wall.*

3.5 Time to re-saturation of the rock wall

A key observation from the previous scenario analysis (Chapter 2) that was later confirmed by the field measurements in BRIE, was the strong de-saturation of the rock matrix next to the deposition hole wall. We present here a global sensitivity analysis of the time needed for the rock to nearly recover from the induced de-saturation, i.e regain saturation levels above 95 %. The corresponding results are presented in Figure 3-4. The time to nearly re-saturate the rock wall, shows a wider distribution than the previous saturation targets in the buffer, from approximately 10 days up to 10^5 days, with a median around 400 days and two cases spreading above 2×10^4 days.

The same four parameters appear at the top of the list of influential parameters as for the saturation of the buffer. The high uncertainty levels around those top parameters and the fact that they induce μ* values of the order of the high end tailing of the CDF seem to indicate that they are involved in parameter interactions. All other parameters except one have sensitivity levels in the middle range of the CDF. These observations point again to a complex prediction sensitive to a great number of parameters likely involved in interaction effects.

3.6 Mass and time at maximum air dissolution in the buffer

Under confined and heterogeneous conditions, pockets of gas can become isolated and subsequently immobilized. One removal pathway under such occurrences is for the air to dissolve into the liquid phase as the pressure increases and then be transported by liquid phase advection and by diffusion (see examples in Chapter 2). In such a case, the removal time of the air introduced with the buffer does not coincide with the saturation time. We argue that an interesting output to analyze in order to assess the fate of the air component introduced with the bentonite buffer is the fraction of the initial air mass getting dissolved at the peak of dissolution as well as the timing of this peak (Figure 3-5 and Figure 3-6). Due to the disparity in porosities between the rock (<0.01) and the bentonite (~0.4), the dominant fraction of the air is found to be present in the bentonite pores. The analysis of the dissolved air content and possible long time residence in liquid phase will thus be focused on the bentonite.

One can see on the CDF in Figure 3-5 that up to approximately 60 % of the initial mass of air introduced with the buffer can remain at the peak dissolution in the liquid phase present in the bentonite under some tested parameter combinations. The median is located around 10 % of the initial air mass undergoing dissolution. The same four parameters inducing the highest sensitivity on the buffer saturation time and rock wall re-saturation are again present as highly influential parameters. One can also see that the gas phase relative permeability parameters β and Γ rank also very high regarding uncertainty of peak air dissolution, which stems naturally from their regulating role on the gas flows before the saturation and pressure have increased to the point where dissolution starts to significantly occur. It is important to note though that these parameters values are subject to high uncertainty as very few measurements were made and reported in the literature. The amount of initial air undergoing dissolution is another prediction subject to high levels of uncertainty spread over a great number of parameters.

Regarding the time to peak air dissolution, one can see in Figure 3-6 that it is approximately one order of magnitude larger than the time required to nearly saturate ¾ of the installed buffer (Figure 3-3). This is consistent with gas forming isolated pockets that eventually get pressurized and undergo dissolution. The air diffusivity in the liquid phase appears to be a high impact parameter (characterized by a large uncertainty) which reflects the action of diffusion against sharp gradients of dissolved air content in the buffer. It has been observed in simulations (see Chapter 2 of this report) that a plume of dissolved air migrates into the rock domain driven by diffusion. The elementary effect related to the gas phase relative permeability coefficient β, also ranks high, which is explained by the fact that it controls the saturation level at which the gas phase practically looses its mobility. The time to peak dissolution in the buffer is also highly sensitive to the four previous high impact parameters z_f, lgK_r, P_{bnd} and p^c_{tunnel} due to their control on the advective flow towards the bentonite (especially the first three). The presence of the fracture and rock porosities in the middle range of sensitivity can be explained by their control on the amount of air migrating to the rock wall during the de-saturation.

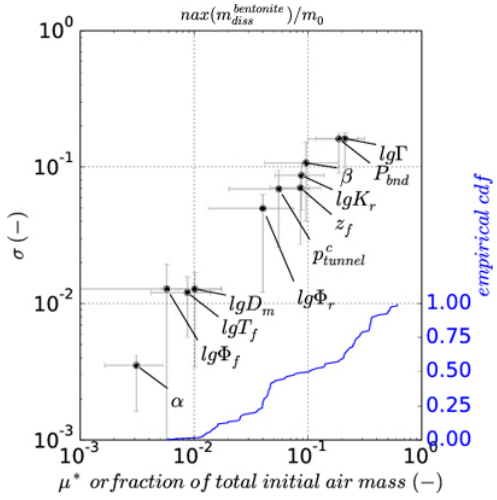

Figure 3-5. *Empirical Cumulative Density Function (blue) and Elementary effect distribution in the (μ*,σ) plane for the fraction of initial air mass undergoing dissolution.*

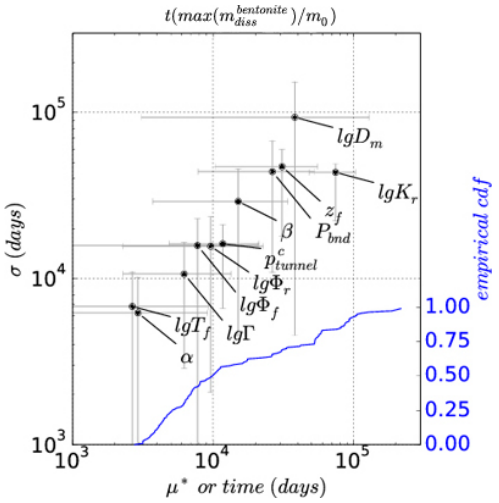

Figure 3-6. *Empirical Cumulative Density Function (blue) and Elementary effect distribution in the (μ*,σ) plane for the time to the dissolution peak.*

3.7 Conclusions and recommendations

This global sensitivity analysis over three types of model output and eleven model parameters has revealed that each model prediction can span a wide range of values for the selected parameter bounds and that the sensitivity structure is complex for all the tested outputs: there are an important number of parameters to which the outputs are simultaneously sensitive and often times with significant parameter interactions and/or non-linearities.

As a consequence, it is difficult to reduce the number of model parameters necessary to predict the time to buffer saturation to a single one or even a limited number of parameters to be assessed in testing a potential deposition hole.

The time to the re-saturation of the rock wall was found to possibly reach several decades and the amount of air getting trapped and dissolved in the buffer has been shown to have a median value of about 10 % of the air mass introduced with the buffer but could also reach up to 60 % of the initial air mass in unfavorable cases which could provide ground to re-assess the initial oxygen levels and margins used in biogeochemical projections in the near canister environment.

4 Site-specific BRIE model

4.1 Objectives

After scoping calculations undertaken for a wide range of operating conditions considered relevant for the future repository in the two previous chapters, this chapter introduces site-specific models of the BRIE site. The objective for this analysis are to assess the gain in prediction of the wetting rate of the bentonite obtained by constraining the rock mass flow model to global open deposition hole inflow rate and by constraining the inflow to identified fracture traces along the deposition hole wall. In the latter case, the influence of the rock matrix permeability close to the wall between the fracture traces is also assessed. The aim is to help determine the usefulness of global inflow rate measurements, characterization of inflow distribution and characterization of local properties for non-fractured wall sections in order to build fitness criteria for future deposition holes.

4.2 Approach

The 2D radial models used in the two previous chapters for scoping scenario and sensitivity analyses were based on simplified geometries which introduced a certain level of abstraction by forcing the use of horizontal fractures and by preventing the design of far field pressure value consistent with the fracture zones and tunnel system.

A set of 3D models encompassing the deposition holes and the rock mass around the BRIE tunnel were developed in an effort to reduce this gap and to make simulations more directly comparable to the BRIE field experiments. A detailed account of the modeling procedure and an extended discussion are available in a separate article (Dessirier et al. 2016) and a PhD thesis (Dessirier 2016).

The general approach was to build a model of the rock mass surrounding the BRIE site starting at the tunnel scale, then introducing refinements to describe the open deposition holes and finally proceed to simulate the introduction of the bentonite columns and their in situ wetting. Each of these three steps is presented in the following sections.

4.3 Tunnel scale model setup

The first step in building a 3D site specific model was a 40×40×40 m cube surrounding the BRIE tunnel (Figure 4-1). The tunnel is represented by internal atmospheric pressure boundary conditions with negligible suction.

Three deformation zones were identified as cutting through this domain and are represented explicitly by 1 m thick planar features with higher conductivities as estimated by hydraulic test (Figure 4-1). Two of these deformation zones, wfrac1 and wfrac2, intersect the tunnel system, the first one near the entrance of the BRIE tunnel. Outer boundary pressures were adopted from a regional model of the Äspö tunnel (Svensson et al. 2008).

We defined 3 homogeneous, isotropic equivalent material types to represent the rock mass between the known fracture zones:

- A skin layer directly around the tunnel where no deformation zone is intersecting.
- Another specific skin layer where wfrac1 and wfrac2 intersect the tunnel.
- A background rock material for the rest of the rock mass.

Groundwater flow is simulated for isothermal conditions and possibly unsaturated conditions in the rock using Richards' equation as implemented in TOUGH2-EOS9.

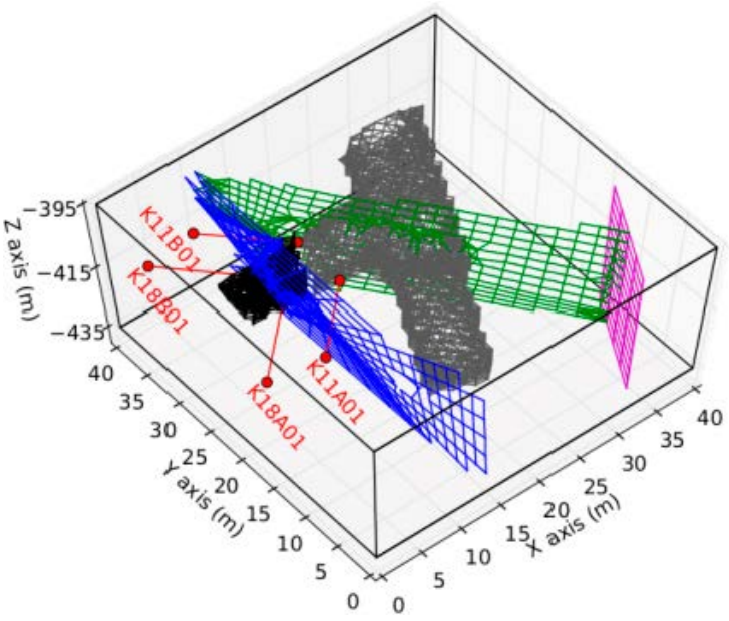

Figure 4-1. *Modeling domain with the end of the TASD tunnel (gray), the BRIE tunnel (black), the known fracture zones: wfrac1 (blue), wfrac2 (green) and NW4 (purple), and the 10-m borehole intervals (red).*

The intrinsic permeabilities for these three materials were fitted by iterative grid search primarily to match the inflow value measured by absorbing mats at the intersection of wfrac1 with the tunnel (78 mL/min), and the aggregated inflow value measured by mats over the rest of the BRIE tunnel floor (24 mL/min).

A secondary target was to approach the pressures recorded in four 10-m long borehole intervals (K11A01: 22.9 bar, K11B01: 3.2 bar, K18A01: 24.8 bar, K18B01: 21.0 bar, see Figure 4-1) drilled in the walls of the BRIE tunnel. It was verified that the fitted material permeabilities are in the range of measurements gathered at the Äspö tunnel in previous projects (Emsley et al. 1997, Vidstrand 2003).

The final retained solution approaches the two inflow targets with less than 5 % difference and the long term pressure values in the borehole intervals with differences under 15 % for the first three of them. The fourth pressure in K18B01 is underestimated by 40 %, which was inherited from the parent model that provided the boundary conditions used for this study. This compromise was used for all model refinements presented in the next section.

4.4 Site-specific open deposition hole models

Based on the previous background tunnel scale model, local refinements were introduced at the emplacement of the two 30cm-diameter BRIE deposition holes (Figure 4-2). No blind prediction of the inflow into the deposition hole was undertaken in this study. Instead three different structural scenarios were defined to represent the walls of the deposition holes:

- One labeled **No_frac**, without fracture, where the rock matrix permeability is fitted to match the measured deposition hole inflow.
- One labeled **K_ave**, with the identified dominant intersecting fracture explicitly modeled in each deposition hole (Figure 4-2) and the rock matrix intrinsic permeability taken as the average of the values measured on borehole core samples retrieved from the BRIE tunnel (1×10^{-20} m^2).
- One labeled **K_low**, with with the identified dominant intersecting fracture explicitly modeled in each deposition hole and the rock matrix intrinsic permeability taken in the low range of the values measured on borehole core samples retrieved from the BRIE tunnel (2×10^{-21} m^2).

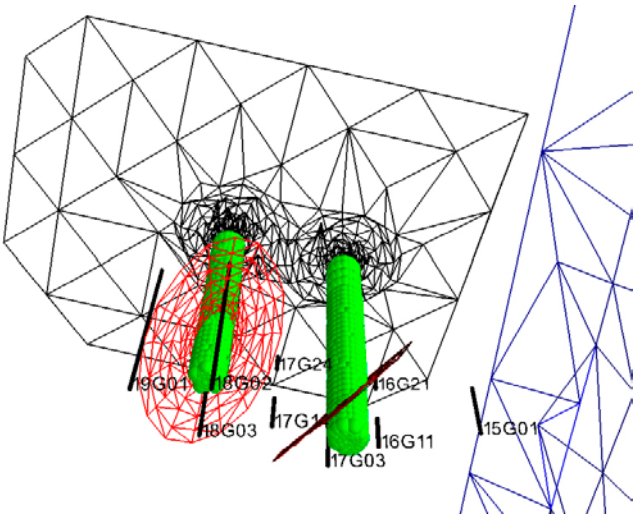

Figure 4-2. *Model geometry in the floor of the BRIE tunnel: deposition holes (green), local fractures (red), wfrac1 (blue), borehole intervals and tunnel floor (black).*

Here again, groundwater flow is represented by isothermal, possibly unsaturated flow as implemented by TOUGH2-EOS9. The deposition hole wall are represented by boundary conditions at atmospheric pressure with negligible suction. Two parameters are fitted simultaneously in each case (either two matrix permeability values in the case of **No_frac,** or two fracture transmissivities in the case of scenarios with fractures, Table 4-1) following an informal grid search. The calibration target was to match the measured deposition hole inflow values of approximately 0.18 mL/min in hole 17 and 0.018 mL/min in hole 18.

Scenario **No_frac** is intended to test the performance of a model based on the global inflow level but without any structural information on the deposition hole rock wall. Scenarios **K_ave** and **K_low** test a case where both inflow value and structural information are available, but with different levels of contribution of the less conductive features, matrix or smaller fractures. Three additional scenarios denoted **No_frac'**, **K_ave'** and **K_low'** where defined for hole 17, where the deposition whole inflow is fitted to 10 times the value measured (so to 1.8 mL/min) in the field in order to test the impact of an overestimation of the inflow in a context where some structural information is available in the form of fracture locations.

Table 4-1. Information summary on modeling scenarios.

Observed inflow Scenarios	**No_frac**	**K_ave**	**K_low**
Local fractures represented?	No	Yes	Yes
Fitting Targets	$q^{17} = 0.18$ mL/min	$q^{17} = 0.18$ mL/min	$q^{17} = 0.18$ mL/min
	$q^{18} = 0.018$ mL/min	$q^{18} = 0.018$ mL/min	$q^{18} = 0.018$ mL/min
Fitting parameters	k_m^{17}, k_m^{18}	T_F^{17}, T_F^{18}	T_F^{17}, T_F^{18}
Fitted values	1.45×10^{-19} m^2,	4.1×10^{-12} m^2/s,	2.35×10^{-11} m^2/s,
	1.8×10^{-20} m^2	1.8×10^{-13} m^2/s	4.2×10^{-13} m^2/s
Fixed values	–	$k_m = 1 \times 10^{-20}$ m^2	$k_m = 2 \times 10^{-21}$ m^2

Increased inflow Scenarios	**No_frac'**	**K_ave'**	**K_low'**
Local fractures represented?	No	Yes	Yes
Fitting Targets	$q'^{17} = 1.8$ mL/min	$q'^{17} = 1.8$ mL/min	$q'^{17} = 1.8$ mL/min
Fitting parameters	$k'_m{}^{17}$	$T'_F{}^{17}$	$T'_F{}^{17}$
Fitted values	1.3×10^{-18} m^2	4.66×10^{-11} m^2/s	2.68×10^{-11} m^2/s
Fixed values	–	$k_m = 1 \times 10^{-20}$ m^2	$k_m = 2 \times 10^{-21}$ m^2

4.5 BRIE bentonite wetting simulations (T8d2–f2)

Following the previously defined scenarios, simulations of the corresponding wetting of unsaturated bentonite columns in each deposition hole were carried out. At this stage, the heterogeneous water delivery along the deposition hole can potentially induced air trapping is some parts of the buffer and/or the de-saturated rock matrix. The isothermal flow of groundwater and air has thus been represented by two-coupled mass balance equation for two components (air and water) distributed in two phases (liquid and gas) as implemented in TOUGH2-EOS3.

The initial 1 mm gap necessary to the installation of the bentonite columns has been neglected and a perfect contact is assumed directly after installation. Also, the two columns have been represented as installed simultaneously, although they were set in place one day apart in the field.

A total of 12 relative humidity sensors W1-12 were installed in the BRIE deposition holes as depicted in Figure 4-3.

The results for all the scenarios are presented along with the translated sensor measurements as the time evolution of saturation at the sensor locations in Figure 4-4. Relative humidity sensor readings h are translated into capillary pressures Pcap using Kelvin's equation (Edlefsen and Anderson 1943): $Pcap = \ln(h).\rho_w.R.T / M_w$ with $\rho_w = 1\,000$ kg/m^3, $R = 8.314$, $T = 288.15$ K and $M_w = 1.8.10^{-2}$ kg/mol, and then translated to saturation levels by means of the inverted retention curve derived for the BRIE bentonite during a laboratory water uptake test: $S_l = (1+(P_{cap}/P_0)^{1/(1-\lambda)})^{-\lambda}$, with $P_0 = 10$ Mpa and $\lambda = 0.28$. Sensor data is represented by crosses in Figure 4-4 while the results from modeling scenarios are represented by different patterned black lines when calibrated against the measured inflows at the BRIE site and gray curves when calibrated one order of magnitude above the field inflow value in hole 17.

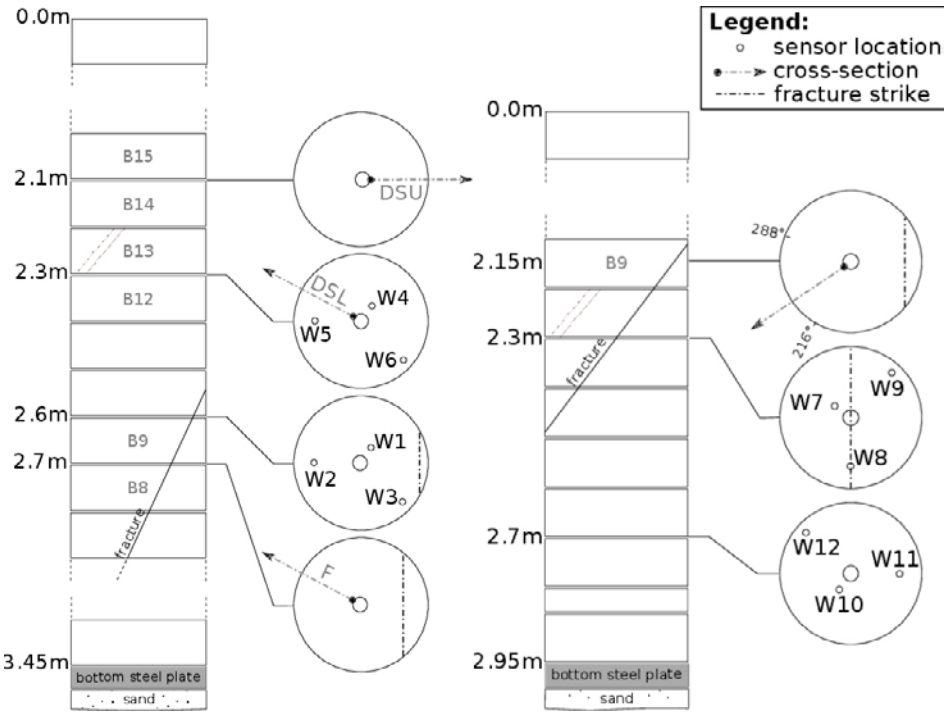

Figure 4-3. *Bentonite column layouts in hole 17 (left) and hole 18 (right). A total of 12 humidity sensors W1-12 were installed at the shown locations. Some cross-section profiles were analyzed right after dismantling following the cross-section line depicted here.*

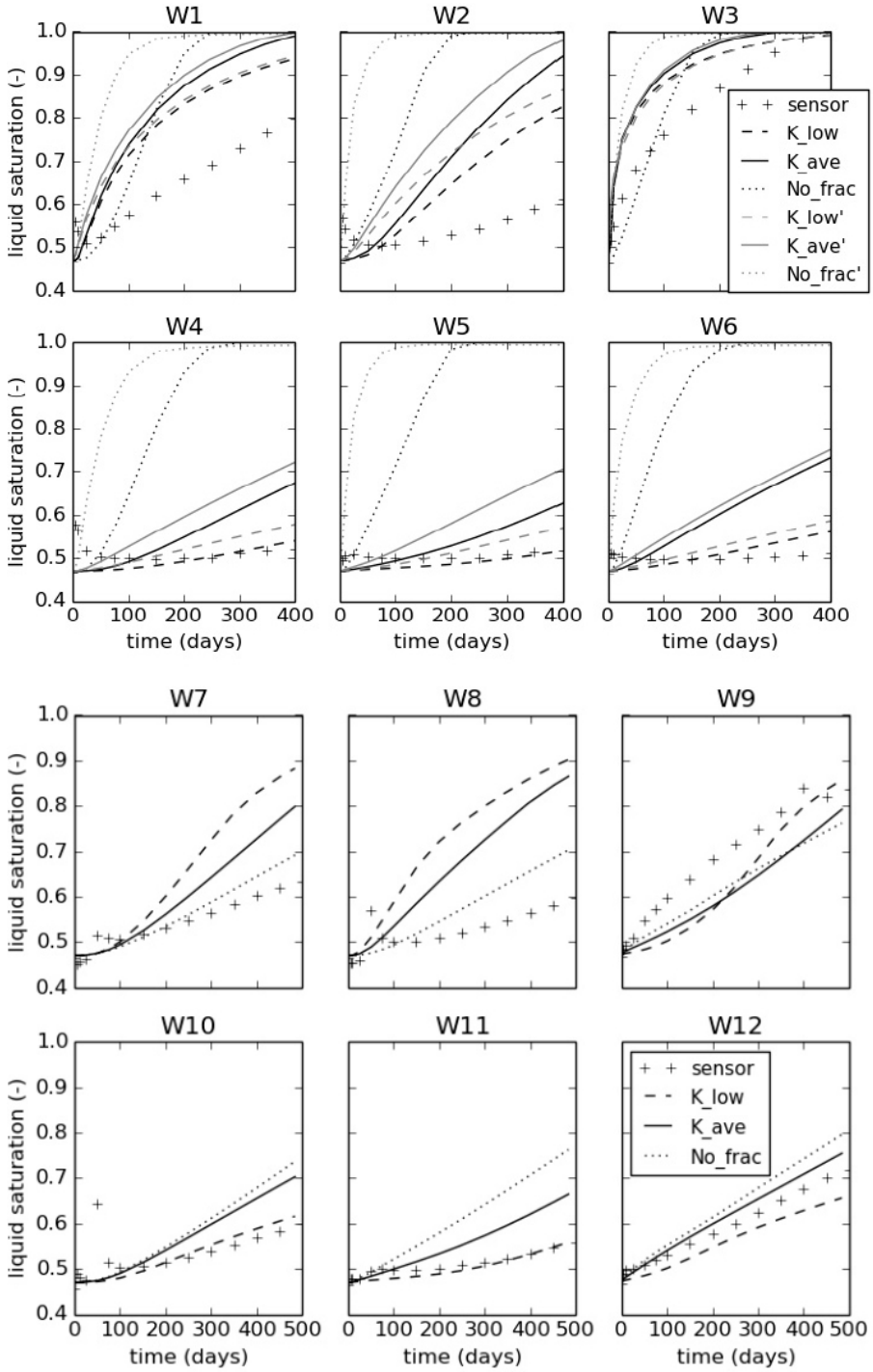

Figure 4-4. *Liquid saturation history translated from relative humidity sensors W1-12 and from modelling scenarios.*

Looking at the data in hole 17 (Figure 4-4-top), one can identify a wet section influenced by the top of the main identified fracture where sensors W1-3 were located and a dry section where W4-6 were located. One can see that all models tend to overestimate the wetting rate and thus the liquid saturation, particularly in the wet section. By looking at the alternative scenarios with 10 times the initial measured inflow in hole 17, one can see that if available the structural information on the location of the flowing fracture seems to influence the model to a greater extent than the exact initial inflow level. Thus in deposition hole where the inflow pattern is dominated by distinct features, the effort should be put on locating these features before estimating their precise inflow contribution. With this level of inflow and domination by a handful of fractures, scenarios without structural information do not provide an adequate response.

Looking at the data in hole 18 (Figure 4-4-bottom), one can see that the sensor responses between the expected wet section with W7-9 and dry section with W10-12 differ less than in hole 17. It is believed in retrospect that the flow in the identified fracture intersection hole 18 was highly channelized and mainly occurring from the top of the fracture trace, and to a lesser extent from the bottom of the fracture trace. This lack of information in the definition of the scenarios would explain the overestimation seen in the wet section of hole 18 and the worsening of the prediction when adopting a lower matrix intrinsic permeability that enhances fracture flow. In contrast with the previous case of hole 17 and due to the lesser difference between the main fracture contribution and the rest of the deposition hole wall, here lumped as matrix, it is conjectured that a threshold deposition hole inflow value (close to that observed in hole 18) could be defined below which information on flowing fracture trace does not help refine the prediction without detailed information on channeling inside the fracture.

The saturation state at the dismantling of BRIE is depicted in Figure 4-5 and Figure 4-6 along three cross-section (in both bentonite and rock) in hole 17 tagged DSU, DSL and F as represented in Figure 4-5 and Figure 4-6-top and along one cross-section in hole 18 (Figure 4-6-bottom). The field data is translated from measurements of water content w and dry density ρ_d on bentonite samples taken after the dismantling using the following equations:

$$\Phi = 1 - \rho_d / \rho_p$$

$$S_l = w \cdot \rho_p / \rho_w \cdot (1 - \Phi) / \Phi$$

assuming a constant water density $\rho_w = 1\,000$ kg/m^3 and a constant solid particle density $\rho_p = 2\,700$ kg/m^3.

The values in the rock are processed from the average of relative humidity measurements made on the dismantled rock wall via Kelvin's equation and a scaled inverted retention curve derived from laboratory measurements on a BRIE core sample. As such the values shown for the saturation in the rock are more uncertain but reveal a de-saturation to levels of at least 0.5 or 0.6 next the bentonite/ rock interface which were hard to sustain in the simulations (Figure 4-5 and Figure 4-6).

The analysis of the cross-sections reveals a lack of detailed understanding of the two-phase flow dynamics occurring in the rock wall. While it was possible to render a strong de-saturation of the rock wall (see Chapter 2), it was generally not possible to sustain this state of de-saturation for the durations after which it was still observed in the field. One possible explanation and formalism to account for a prolonged de-saturation could be to include a description of hysteresis effects in the rock wall which would slow down the re-saturation. This avenue is only conjectured at this point and will be explored in future modeling attempts. While it appears that the liquid permeability in the rock is over-estimated, it is not entirely clear if and to which extent this overestimation should be reflected on the intrinsic and/or relative permeability. Based on the high reproducibility of laboratory water uptake tests on bentonite blocks of the same size as those used in BRIE (Vidstrand et al. 2017), it is assumed that the over-estimation of the saturation in the bentonite is mainly caused by the lack of understanding and limited description of the flowing structures and unsaturated flow phenomena in the surrounding rock mass.

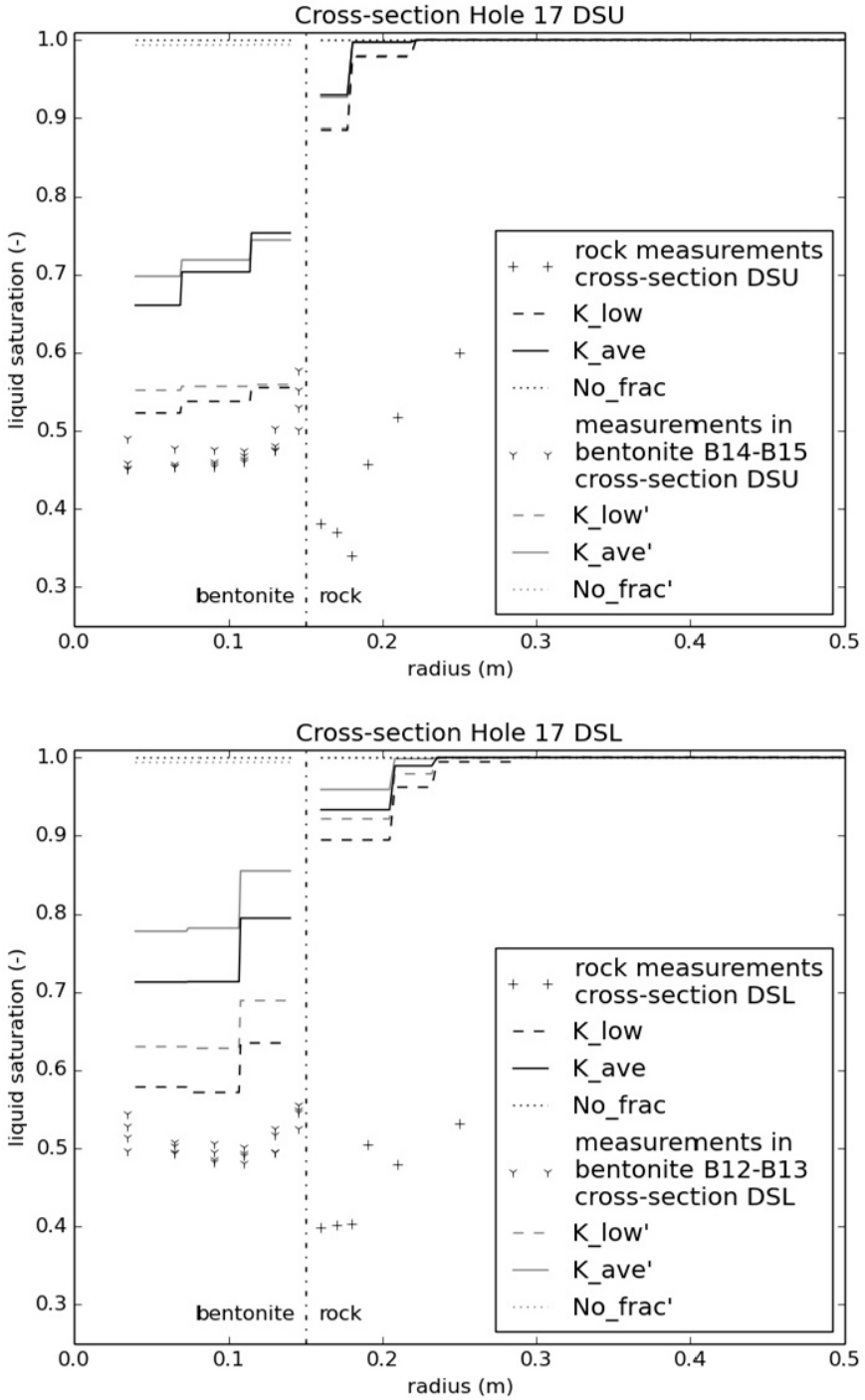

Figure 4-5. *Liquid saturation profile in bentonite and rock wall around hole 17 along the two cross-sections DSU and DSL at time of dismantling (419 days): Models and measurements.*

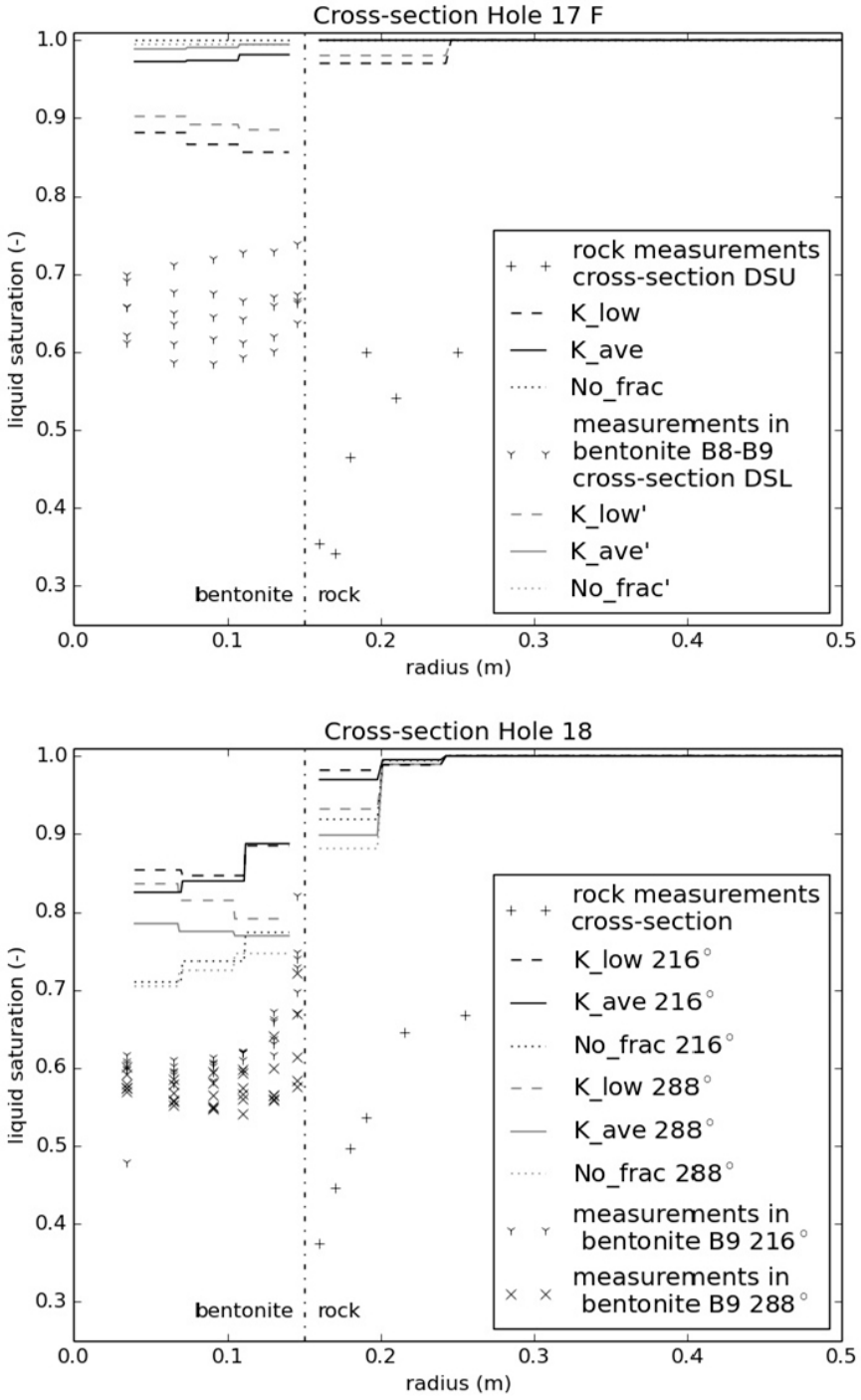

Figure 4-6. *Liquid saturation profile in bentonite and rock wall along one cross-section in hole 17 "F" at t = 419 days and in hole 18 at t = 518 days: Models and measurements.*

4.6 Conclusions and recommendations

3D modeling scenarios of BRIE deposition holes revealed a limited degree of understanding in selecting and describing the main structural features contributing to the bentonite water uptake. Generally it is found that the heterogeneity of the rock mass has a strong regulating effect on the flow rates observed during bentonite wetting and consequently homogeneous models consistently give low estimates of the buffer wetting time. Detailed information on the location of inflow points and traces seems more effective to constrain the predictions of wetting time than open-hole aggregated inflow rate measurements.

More specifically, in cases such as hole 17, where the open hole inflow seems clearly dominated by a reduced number of fractures, detailed information on the location of the flowing fracture traces seems to take priority over quantifying the exact inflow into the deposition hole. In cases such as hole 18, where the inflow seems to be lower and more distributed, it appeared harder to refine the prediction using planar fractures with uniform transmissivity (i.e without information on the local channeling effects).

In both cases, analyses of dismantled rock wall samples revealed a lack of understanding of the re-saturation dynamics in the rock wall. A possible explanation could be a strong hysteresis effect that introduces a gas residual saturation and slows down the re-saturation process. This type of effect is an interesting hypothesis to test in future modeling attempts.

Following these observations and if the buffer wetting time is considered critical for the safety of the KBS-3 method, it is recommended to include spatial inflow point characterization into the criteria used to assess the fitness of a potential deposition hole.

5 Bentonite photograph analysis

The bentonite parcel from BRIE hole 18 could be retrieved in one piece and without significant surface damage which allowed a very detailed photo-documentation of the surface where the gray tones reveal many fracture traces that seem to have provided groundwater to the bentonite buffer. The objective with this analysis was to produce a quantitative reconstruction of the water content on the whole bentonite parcel surface incorporating both the structural information from the gray tones of the photo-documentation and the physical bentonite sampling (water content) at selected points. Such a reconstruction can in turn shed light on the relative importance of features regarding groundwater inflow and thus help constrain numerical models.

5.1 The dismantling photo-documentation

The dismantling photographs (such as Figure 5-1) show different gray scale patterns that appeared at first inspection to be correlated with the water content of near the bentonite surface. For example, the inclined gray line in blocks 5 to 8 at the center of the picture in Figure 5-1 corresponds to a known flowing fracture trace. Other features, like the subvertical feature at the bottom of the photograph across blocks 1 to 6 could be hypothesized as a drilling-induced tensile fracture. It has thus been proposed to explore the correlation between the gray value of the dismantling photographs in order to investigate its potential in helping achieve a high-resolution surface reconstruction of the water content of the bentonite in BRIE hole 18.

Figure 5-1. *Example of dismantling photograph for hole 18 (credits: Mattias Åkesson).*

5.2 The bentonite samples

Details of the sampling scheme can be found in Fransson et al. (2017). The samples nearest to the bentonite surface (1cm deep from the outer surface and 1.5cm in radius) are represented on top of a panorama of the bentonite surface gray values extracted from the different photographs (Figure 5-2). A more detailed account of the procedure employed to process the photographs into unfolded regions of the surface of the bentonite column is available in Dessirier et al. (2017).

Figure 5-3 shows the correlation between the gray value of the background panorama in Figure 5-2 against the liquid saturation measured for the sampled volumes near the bentonite surface. The coefficient of determination of the regression is equal to 0.48, and the hypothesis of a regression slope being equal to zero is rejected with a risk value well below 1 %, which points to the fact that the photographs contain some structural information to help determine the saturation state of the bentonite near its surface. The residual between the measured value and the regression line is hard to neglect though, instead it was proposed to assume that the residual arises from a stationary process and can be spatially interpolated by kriging. More details on the formalism and the complete set of equations are available in Dessirier et al. (2017). The intermediary step: regression and kriging of the residual are presented in Figure 5-4a,b. The complete reconstruction, i.e the sum of the regression and the kriging of residuals is shown in Figure 5-4c alongside the kriging variance (Figure 5-4d) that provides an estimation of the prediction error.

The regression-kriging procedure based on the dismantling photographs capture more features influencing the groundwater inflow at the bentonite/rock interface than traditional interpolation methods based solely on points measurements, e.g inverse-distance interpolation (Figure 5-5 given as a reference). The sinusoidal trace between z=0.4 m and z=0.8 m in Figure 5-4c is one example of feature captured in the regression-kriging reconstruction that corresponds to a previously characterized inflowing fracture. The results from the reconstruction also seem to reveal information on the in-plane channeling in the fracture, i.e in this case the presence of a more conductive or better connected channel intersecting the deposition hole at the top of the trace. The regression-kriging analysis also reveals vertical conductive features (at R.θ=0.05, 0.3, 0.55 and 0.8 m approximately) possibly related to stress effects.

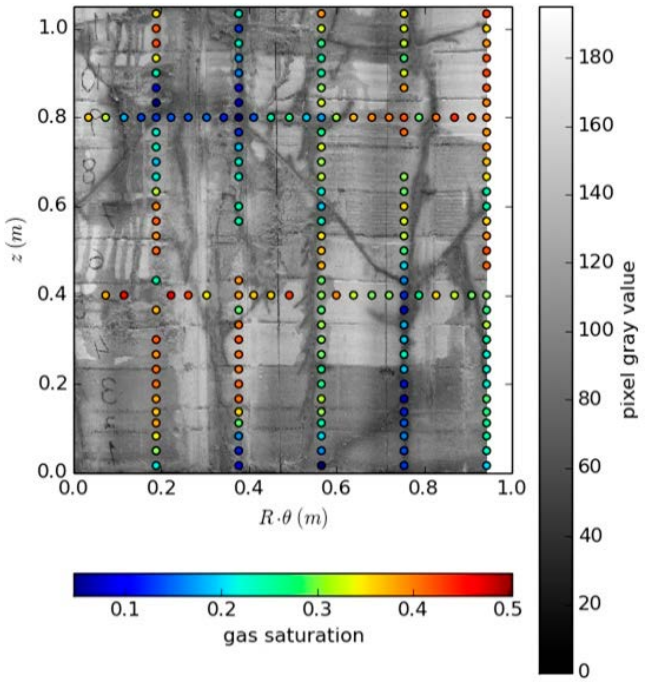

Figure 5-2. *Overlay of the assembled panorama of gray scale unfolded surface elements retrieved from dismantling photographs (background) and translated gas saturation from measurements on samples (colored dots).*

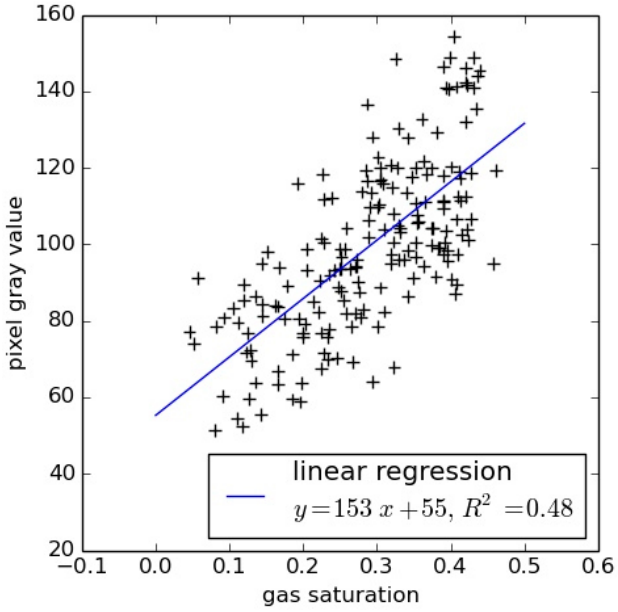

Figure 5-3. *Correlation plot between surface sample and local gray value from dismantling photographs.*

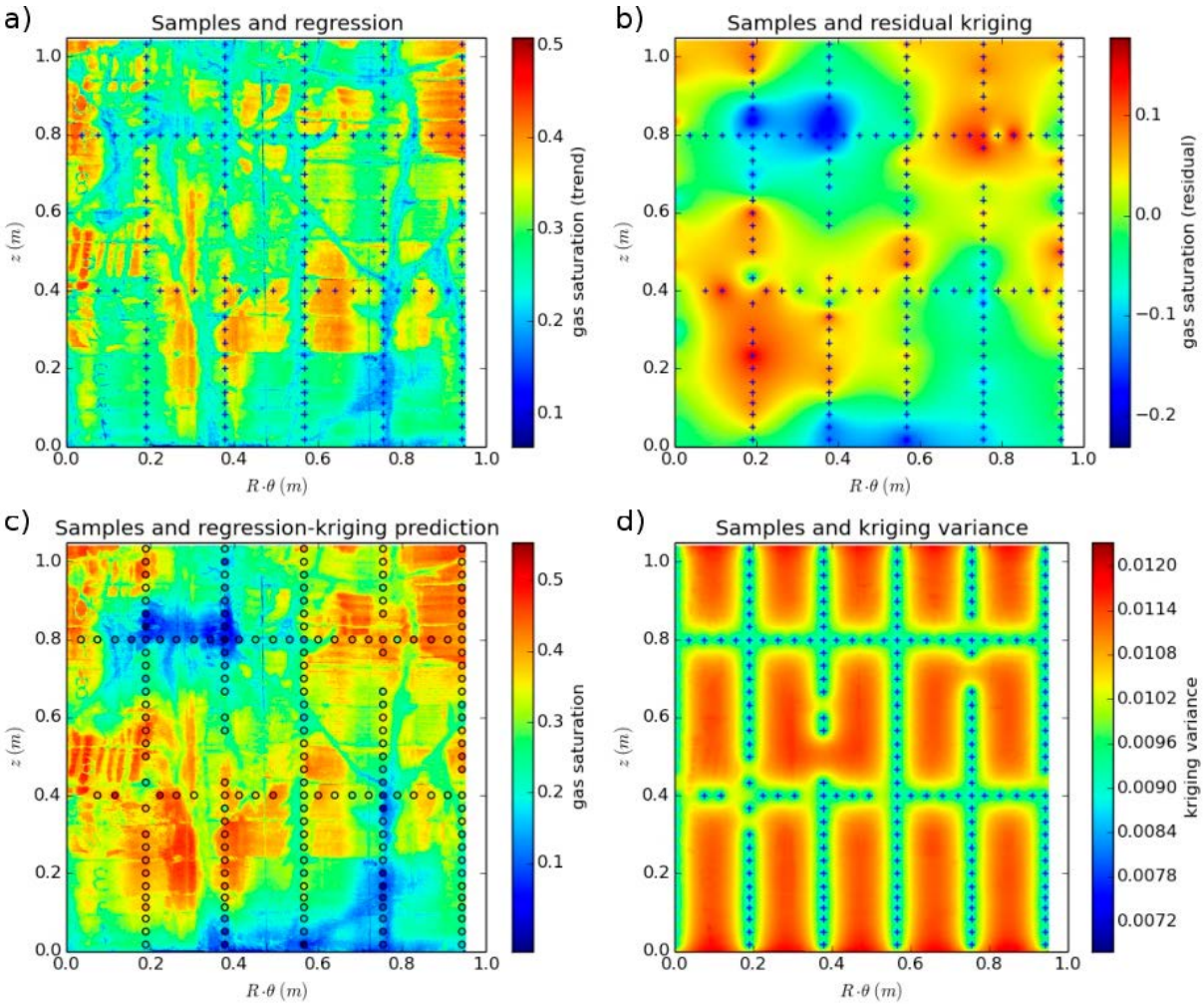

Figure 5-4. *Unfolded bentonite surface reconstruction of gas saturation by regression-kriging: regression (a), kriging of residuals (b), regression-kriging prediction (c) and kriging variance (d).*

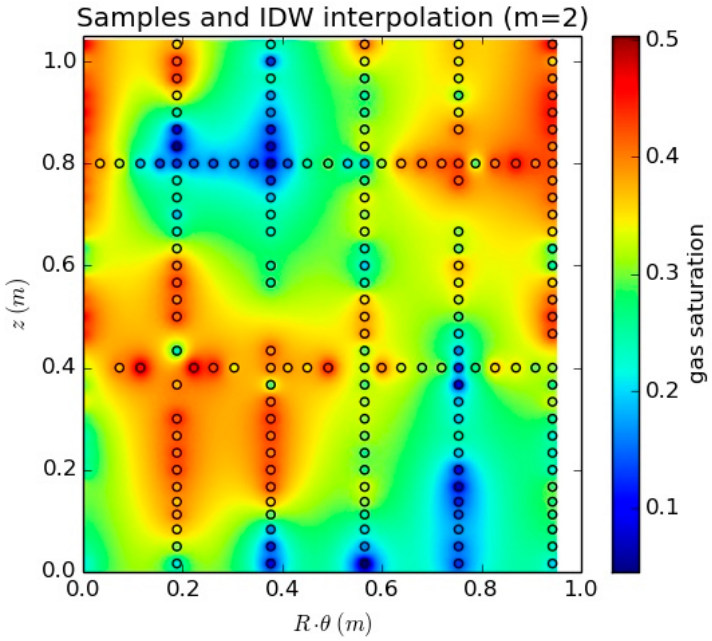

Figure 5-5. *Unfolded bentonite surface reconstruction of gas saturation by inverse distance weighting interpolation (exponent value = 2).*

It is worthwhile noting that although it accounts for errors or deviations from the regression line in a statistical sense, the residual term could stem from various origins among which are: possible errors in extracting/referencing the surface texture from the photographs, to a possible difference between 1 cm-thick surface samples and purely superficial gray value, to unregistered surface damage or even perturbation by drilling water migration or during transport. A more extensive discussion of the sources of error is available in Dessirier et al. (2017).

Although not included in the original sampling plan, the dismantling photographs obtained for BRIE hole 18, made it possible to propose a high-resolution reconstruction of the saturation state at the surface of the bentonite previously in contact with the rock wall by developing an ad-hoc regression-kriging procedure. Such a reconstruction can help gain qualitative insight in the type of rock features that influenced the bentonite wetting process and their respective degree of contribution to the water delivery at the bentonite/rock interface. It could also be used as a distributed map of saturation to be used in future model inversions to increase our understanding of the relative importance of different types of rock features with regard to buffer wetting.

6 Summary and conclusions

6.1 Summary – overall approach

We investigate effects of two-phase flows in the near-canister domain using numerical modeling.

In a first set of simulations using simplified 2D radial geometries, different conceptualizations of unsaturated flow are compared, namely (i) simplified unsaturated groundwater flow according to Richards' equation where only liquid water is physically accounted for, and (ii) two-phase flow theory where both water and air are each subject to mass balance constraints. Impacts of different possible locations of intersecting rock fractures are also investigated. Two modules of the TOUGH2 code are used:

- One including full air/water two-phase dynamics (base case eos3).
- One using the common Richards' assumptions that neglects the air mass balance and simply solves the liquid moisture transport (case eos9).

Through a global sensitivity analysis, we also investigated the time to near buffer saturation, the rock wall re-saturation time and the potential for air dissolution as well as its timing.

At a later stage and with site-specific 3D models calibrated to respect tunnel and deposition hole inflows, we attempted to capture the wetting dynamics of the buffer columns inserted in rock deposition holes during the BRIE experiment.

Additional analyses on measured samples and photo-documentation of the dismantling of the BRIE experiment were also performed in order to gain insight into the dominant rock features influencing the in situ buffer wetting process.

6.2 Conclusions

- The installation of a bentonite buffer can cause considerable de-saturation of the adjacent rock matrix, which can be captured by some parameter combinations and is supported by field evidence.
- The position of the fracture(s)/deposition hole intersection(s) can considerably influence the buffer saturation times.
- The aggregated open deposition hole inflow value does not help significantly constrain the buffer wetting time without information on the spatial distribution of the inflow points.
- Locating the dominant inflow points and traces is the most effective type of information to constrain the wetting time prediction.
- Richards' equation systematically predicts higher degrees of saturation and shorter re-saturation times than the model with full two-phase flow representation.
- The under-prediction made by Richards' equation were relatively small (10–15 %) at lower water saturations.
- The under-prediction made by Richards' equation increases as the system approaches saturation; underestimations in estimating times to reach full (or near-full) water saturations were considerable.
- The modeled reduction (from 64 % to 1–2 % within the first two years) of the separate gas phase initially present in the unsaturated bentonite buffer could not be explained by gas leaving the system to the tunnel via the unsaturated pore space. Instead, a significant part of the gas may dissolve into the relatively immobile liquid phase and remain for decades or more in the vicinity of the deposition hole.
- Elevated concentrations of dissolved oxygen resulting from such dissolution occurrences may influence geochemistry and microbial growth.

6.3 Open Issues

Examples of remaining open issues, (presented in decreasing order of importance):

- Occurrence and impacts of de-saturation of the rock domain in the near-canister region that can follow after installation of bentonite in the deposition hole, with potential hysteresis effects.
- Possible effects of (uncertain) background fracture networks and statistics and the effect of in-plane channelling/fracture roughness.
- Influence of biological and geochemical processes on residence times of air dissolved in water.
- Parameterization of the decrease in gas relative permeability at high saturations and possible residual gas saturation.
- Possible questioning of the concept of intrinsic permeability for bentonite.
- Influence (on two-phase flow processes) of mechanisms that are highly sensitive to heterogeneity, in particular to fracture roughness and porosity of the mineral structure constituting the rock matrix.
- Uncertainties in estimating re-saturation times, in particular in estimates to reach high water saturations (>98 %), where two phase flow dynamics – that cannot be modeled using Richards' equation – may play an important role.
- Open questions remain regarding bubble trapping dynamics and dissolution rates; the time to reach full saturation may be influenced (or governed) by dissolution of residual gas and/ or trapped gas bubbles.
- Potential for and dynamics of transport of substances from rock to bentonite, e.g. given uncertain impacts of gas phase residuals.
- Parameterization of the molecular diffusion of dissolved air in groundwater.

6.4 Comments and Recommendations

It is envisaged that additional scenario-based uncertainty analyses will be needed in order to investigate the potential time-scales for buffer saturation, and potential transport pathways from rock to bentonite (which may occur as a result of low water pressures in the bentonite). Developing and applying strategies for adopting stochastic uncertainty analysis may also be needed. Either way, such analyses and developments should serve as a basis for BRIE experiment interpretation, as well as for extending beyond BRIE prediction experiments. The particular setting of the TASO tunnel and BRIE experiments only represents one or a few settings ('realizations') of the reality in which canister deposition holes may exist in a future repository scenario. Therefore, adopting uncertainty-based scenario analysis may serve as a basis for investigating possible canister deposition hole settings and realistic expectations of the re-saturation behavior of fractured rock in other, similar fractured rock settings.

Neglecting two-phase flow dynamics like air dissolution adds significant uncertainty in the estimated times to buffer saturation and more so as one gets nearer to full saturation. As a consequence, attention should be paid to detailed modeling of two-phase flow dynamics in the near-canister domain, e.g. characterizing unsaturated flows at points of intersection of the deposition holes with the surrounding fracture network.

Regarding robust criteria for deposition hole siting, a possible issue is whether or not, or to which extent, the geometry of the fracture / deposition hole intersections should be considered. For instance, present results show that effects of fracture position on buffer saturation times can be considerable, with differences up to 2 orders of magnitude (Figure 3-3 e.g) in the investigated cases.

A more open and fundamental question is the ultimate fate of the air included in the bentonite at installation. Exploratory scenarios laid out here showed that a significant part of the air could in fact undergo dissolution instead of migrating out of the deposition hole as a separate gas phase. The gas may then dissolve into a relatively immobile liquid phase and remain for decades or more in the vicinity of the deposition hole. This possibility implies in principle that biogeochemical processes could be triggered and become important for the performance of the repository. Therefore, in order to understand the implications of such an extended presence of gas saturated water, present results may need to be related to geo-biological and geochemical models.

References

SKB's (Svensk Kärnbränslehantering AB) publications can be found at www.skb.com/publications.

Alonso E E, Alcoverro J, Coste F, Malinsky L, Merrien-Soukatchoff V, Kadiri I, Nowak T, Shao H, Nguyen T S, Selvadurai A P S, Armand G, Sobolik S R, Itamura M, 2005. The FEBEX benchmark test: case definition and comparison of modelling approaches. International Journal of Rock Mechanics and Mining Sciences 42, 611–638.

Campolongo F, Cariboni J, Saltelli A, 2007. An effective screening design for sensitivity analysis of large models. Environmental Modelling & Software 22, 1509–1518.

Chasset C, Jarsjö J, Erlström M, Cvetkovic V, Destouni G, 2011. Scenario simulations of CO_2 injection feasibility, plume migration and storage in a saline aquifer, Scania, Sweden. International Journal of Greenhouse Gas Control 5, 1303–1318.

Croucher A, 2011. PyTOUGH: a Python scripting library for automating TOUGH2 simulations. In Proceedings of the 33rd New Zealand Geothermal Workshop, Auckland, New Zealand, 21–23 November 2011 (Vol. 21, p e23).

Cussler E L, 1997. Diffusion: mass transfer in fluid systems. 2nd ed. Cambridge: Cambridge University Press.

Dessirier B, 2016. Numerical modeling of groundwater and air flow between compacted bentonite and fractured crystalline rock. PhD thesis. Stockholm University, Sweden.

Dessirier B, Jarsjö J, Frampton A, 2014. Modeling two-phase-flow interactions across a bentonite clay and fractured rock interface. Nuclear Technology 187, 147–157.

Dessirier B, Frampton A, Jarsjö J, 2015. A global sensitivity analysis of two-phase flow between fractured crystalline rock and bentonite with application to spent nuclear fuel disposal. Journal of Contaminant Hydrology 182, 25–35.

Dessirier B, Frampton A, Fransson Å, Jarsjö J, 2016. Modeling early in situ wetting of a compacted bentonite buffer installed in low permeable crystalline bedrock. Water Resources Research 52, 6207–6221.

Dessirier B, Åkesson M, Lanyon B, Frampton A, Jarsjö J, 2017. Reconstruction of the water content at an interface between compacted bentonite blocks and fractured crystalline bedrock. Applied Clay Science 142, 145–152.

Dueck A, Börgesson L, 2007. Model suggested for an important part of the hydro-mechanical behaviour of a water unsaturated bentonite. Engineering Geology 92, 160–169.

Edlefsen N E, Anderson A B, 1943. Thermodynamics of soil moisture. Berkeley, CA: University of California.

Emsley S, Olsson O, Stenberg L, Alheid H-J, Falls S, 1997. ZEDEX – A study of damage and disturbance from tunnel excavation by blasting and tunnel boring. SKB TR 97-30, Svensk Kärnbränslehantering AB.

Finsterle S, Pruess K, 1995. Solving the estimation-identification problem in two-phase flow modeling. Water Resources Research 31, 913–924.

Frampton A, 2010. Stochastic analysis of fluid flow and tracer pathways in crystalline fracture networks. PhD thesis. Royal Institute of Technology, Stockholm, Sweden.

Fransson Å, Åkesson M, Andersson L, 2017. Bentonite Rock Interaction Experiment. Characterization of rock and installation, hydration and dismantling of bentonite parcels. SKB R-14-11, Svensk Kärnbränslehantering AB.

Jarsjö J, Destouni G, 1998. Groundwater degassing in fractured rock: Modeling and data comparison. SKB TR-98-17, Svensk Kärnbränslehantering AB.

Jarsjö J, Destouni G, 2000. Degassing of deep groundwater in fractured rock around boreholes and drifts. Water Resources Research 36, 2477–2492.

Jarsjö J, Destouni G, Gale J, 2001. Groundwater degassing and two-phase flow in fractured rock. Summary of results and conclusions achieved during the period 1994–2000. SKB TR-01-13, Svensk Kärnbränslehantering AB.

Leverett M C, 1941. Capillary behavior in porous solids. Transactions of the AIME 142, 152–169.

Liu H H, Bodvarsson G S, 2001. Constitutive relations for unsaturated flow in a fracture network. Journal of Hydrology 252, 116–125.

Liu H-H, Li L, Birkholzer J, 2012. Unsaturated properties for non-Darcian water flow in clay. Journal of Hydrology 430–431, 173–178.

Millington R J, Quirk J P, 1961. Permeability of porous solids. Transactions of the Faraday Society 57, 1200–1207.

Morris M D, 1991. Factorial sampling plans for preliminary computational experiments. Technometrics 33, 161–174.

Pruess K, Oldenburg C M, Moridis G J, 1999. TOUGH2 user's guide, version 2.0. Berkeley, CA: Lawrence Berkeley National Laboratory.

Rutqvist J, Ijiri Y, Yamamoto H, 2011. Implementation of the Barcelona Basic Model into TOUGH–FLAC for simulations of the geomechanical behavior of unsaturated soils. Computers & Geosciences 37, 751–762.

Svensson U (ed), Vidstrand P, Neretnieks I, Wallin B, 2008. Towards a new generation of flow and transport models for the Aespoe Hard Rock Laboratory. Main results from the project Äspö models 2005. SKB R-08-74, Svensk Kärnbränslehantering AB.

Tong F, Jing L, Zimmerman R W, 2010. A fully coupled thermo-hydro-mechanical model for simulating multiphase flow, deformation and heat transfer in buffer material and rock masses. International Journal of Rock Mechanics and Mining Sciences 47, 205–217.

Vidstrand P, 2003. Äspö Hard Rock Laboratory. Update of the hydrogeological model 2002. SKB IPR-03-35, Svensk Kärnbränslehantering AB.

Vidstrand P, Åkesson M, Fransson Å, Stigsson M, 2017. Task 8 of SKB Task Forces EBS and GWFTS: Modelling the interaction between engineered and natural barriers – An assessment of a fractured bedrock description in the wetting process of bentonite at deposition tunnel scale. A compilation of Task 8 descriptions. SKB P-16-05, Svensk Kärnbränslehantering AB.

Yang C, Samper J, Molinero J, Bonilla M, 2007. Modelling geochemical and microbial consumption of dissolved oxygen after backfilling a high level radiactive waste repository. Journal of Contaminant Hydrology 93, 130–148.

Åkesson M, Kristensson O, 2008. Mechanical modeling of MX-80 – Development of constitutive laws. Physics and Chemistry of the Earth, Parts A/B/C 33, S504-S507.

Arkitektkopia AB, Bromma, 2017

SKB is responsible for managing spent nuclear fuel and radioactive waste produced by the Swedish nuclear power plants such that man and the environment are protected in the near and distant future.

skb.se